NTNU

Norwegian University of
Science and Technology

Experimental and numerical kinetic study on charged and excited species in oxyfuel combustion for CO2 capture

Krzysztof Adam Grabinski

Experimental and numerical kinetic study on charged and excited species in oxyfuel combustion for CO2 capture

Author:

Krzysztof GRABINSKI

Supervisor at NTNU:
Nils Erland L. HAUGEN

Supervisor at SUT:
Andrzej SZLEK

Supervisor at SINTEF:
Mario DITARANTO

NTNU

Norwegian University
of Science and Technology

Department of Energy
and Process Engineering

MASTER THESIS

for

Student Krzysztof Grabiński
Spring 2016

Experimental and numerical kinetic study on charged and excited species in oxyfuel combustion for CO2 capture

Eksperimentelle og numeriske studier av ladede og ioniserte stoff i oxyfuel forbrenning for CCS

Background and objective

In recent years, it has become more and more clear that the majority of the observed climate change is man-made. This calls for a radical change in energy production and consumption. A shift to renewable and nuclear energy sources, together with low emission fossil fuel technologies and a reduced energy consumption, constitute possible ways of transforming the global energy mix into a more environmentally friendly composition. Despite many possibilities, fossil fuels will maintain a major role in the global energy production for the foreseeable future. It is therefore crucial to develop CO2 free and efficient technologies for fossil fuel energy conversion.

Within the scope of the project, selected issues in chemical kinetics of flames will be investigated. The first part describes numerical analysis of high temperature combustion products as a working fluid in a magnetohydrodynamic generator (MHD). An MHD generator is a thermodynamic system where heat is converted directly to electrical energy, without any moving parts. The MHD generator utilizes the effect of interaction between the product of natural ionization of the flame and a stationary magnetic field. As a consequence of the interplay, electric power is produced.

In the light of a stronger emphasis on carbon dioxide emission and the need for energy production with Carbon Capture and Storage (CCS), the idea of MHD must be re-assessed. There are three main technologies for capturing carbon dioxide, namely pre-combustion, post-combustion and oxyfuel combustion capture. The focus of this thesis will be on oxyfuel combustion capture, in which the fuel is combusted in an atmosphere consisting of only oxygen and CO2, such that the exhaust is essentially composed of CO2 and steam when the oxygen excess ratio is close to unity. From this, the CO2 is easily captured by condensing out the steam. Burning the fuel in almost pure oxygen gives an opportunity to obtain a high temperature flame in near plasma conditions, which is characterized by a higher value of electrical conductivity due to chemical ionization of the flame. Hence, there is a possibility to combine CCS oxyfuel combustion technology with a MHD process resulting in a high efficient combined cycle MHD power plant with low carbon dioxide emission. The potential of the concept will be evaluated based on a chemical kinetic study.

In addition to ionized species produced during the combustion reactions, excited species responsible for the electromagnetic emission of flames are also formed. This process, called chemiluminescence, is also temperature dependent, hence particularly important in oxyfuel

combustion. The kinetic study will therefore be extended to add all intermediate reactions of chemiluminescence in the numerical calculations, and experiments in methane - oxygen flames diluted with CO2 and N2 will be conducted to validate the simulations.

The study will provide a better understanding of the role of species in excited state in oxyfuel combustion kinetics and the possible dependency between the concentration of excited species in the flame and the content of electrically charged particles can be checked. This work will also assess the potential of optical emission measurement as a tool for flame control and monitoring in industrial applications.

The work of this Master thesis is linked to the SINTEF Energi projects MOCCA (Polish-Norwegian Research Programme Contract No Pol-Nor/232738/101/2014) and the BIGCCS Centre (Research Council of Norway - FME Contract No 193816/S60).

The following tasks are to be considered:

1. Literature review on MHD technology and chemiluminescence measurement techniques.
2. Numerical analysis of selected plasma properties with a special focus on electric conductivity
3. Examination of chemiluminescence kinetic models.
4. Training in HSE for the use of laboratory and combustion experiments
5. Installation of a test setup for chemiluminescence measurements
6. Establish a plan for experimental work
7. Training in spectrometry of flames and spectrally resolved optical measurements
8. Perform the experimental campaign
9. Data processing and analysis of results.
10. Summary and final conclusions.
11. Make a scientific draft paper gathering the main results and conclusions from the thesis
12. Make proposal for further work

-- " --

Within 14 days of receiving the written text on the master thesis, the candidate shall submit a research plan for his project to the department.

When the thesis is evaluated, emphasis is put on processing of the results, and that they are presented in tabular and/or graphic form in a clear manner, and that they are analysed carefully.

The thesis should be formulated as a research report with summary both in English and Polish, conclusion, literature references, table of contents etc. During the preparation of the text, the candidate should make an effort to produce a well-structured and easily readable report. In order to ease the evaluation of the thesis, it is important that the cross-references are correct. In the making of the report, strong emphasis should be placed on both a thorough discussion of the results and an orderly presentation.

The candidate is requested to initiate and keep close contact with his/her academic supervisor(s) throughout the working period. The candidate must follow the rules and regulations of NTNU as well as passive directions given by the Department of Energy and Process Engineering.

Risk assessment of the candidate's work shall be carried out according to the department's procedures. The risk assessment must be documented and included as part of the final report. Events related to the candidate's work adversely affecting the health, safety or security, must be documented and included as part of the final report. If the documentation on risk assessment represents a large number of pages, the full version is to be submitted electronically to the supervisor and an excerpt is included in the report.

Pursuant to "Regulations concerning the supplementary provisions to the technology study program/Master of Science" at NTNU §20, the Department reserves the permission to utilize all the results and data for teaching and research purposes as well as in future publications.

The final report is to be submitted digitally in DAIM. An executive summary of the thesis including title, student's name, supervisor's name, year, department name, and NTNU's logo and name, shall be submitted to the department as a separate pdf file. Based on an agreement with the supervisor, the final report and other material and documents may be given to the supervisor in digital format.

☒ Work to be done in lab (Thermal engineering lab)

Department of Energy and Process Engineering, April 1th 2016

Prof. Olav Bolland
Department Head
e-mail: olav.bolland@ntnu.no

Prof. Nils Erland L Haugen
Academic Supervisor
e-mail: nilshau@ntnu.no

Dr. Mario Ditaranto, SINTEF Energi
Co-advisor
e-mail: mario.ditaranto@sintef.no

Abstract

Global climate change enforce the new approach in the energy production and consumption sector. Despite many possibilities, fossil fuels will remain the main primary energy source. It is, therefore essential to develop new technologies to reduce the man-made influence on the environment.

The aim of this thesis is to investigate selected issues of the oxy-fuel combustion process and the flame chemical kinetics. First part contains a numerical investigation of the plasma conductivity from the Magnetohydrodynamic (MHD) Power Plant perspective. For that purpose, the chemical mechanism including ions and electrons was developed. The second part describes the experimental and numerical study of chemiluminescence phenomena involving the generation process of chemically excited species. It allowed to create the chemical mechanism, which describes the creation of both electrically and chemically excited particles.

Acknowledgments

Contents

List of Figures

List of Tables

x

1 Study of high temperature plasma

1.1 Theoretical framework

Plasma which properties are investigated in this work can be used in MHD generators as a working fluid. Before going into the details about calculations that were carried out for the purpose of this work, it is necessary to explain the idea of a magnetohydrodynamic generator and the relation to oxy-fuel combustion.

The magnetohydrodynamic power generation has its origin in Faraday's law of induction, first discovered in 1831 [1]. According to the law, which is a fundamental rule for many types of generators and electrical motors, there is an interaction between an electric circle and a magnetic field, resulting in production of an electromotive force called an electromagnetic induction. In January 1832, Michael Faraday set up a primitive MHD generator on Waterloo Bridge in London [2]. He assumed that electrically conductive water passing through the earth's magnetic field should produce electromotive force. Despite the fact that this experiment was not successful, his attempts lay the groundwork for future development of magnetohydrodynamic power generation.

The underlying principle of a MHD generator is, therefore, simple. Electromagnetic induction occurs when a moving conductive material cuts the lines of a stationary magnetic field. As a consequence an electric field is set up such that electric power can be produced. In alternative current electric generators, where mechanical energy is converted to electric energy, the conductive material is a cooper wire, formed as a coil. The cooper wire coil rotates inside the magnetic field, cutting its lines and an alternating current is generated. In the MHD generator, on the other hand, a fluid conductor is employed instead of a solid conductive material. There is, therefore, no mechanical energy involved and a heat energy in the form of electrically conductive fluid is converted directly into electric energy. Fig. 1.1 presents the fundamental principle of operation for an MHD generator.

Basically, the MHD generator is a heat engine in which an electrically conductive fluid expands against the Lorentz force due to a magnetic field. The magnetic field, characterized by the magnetic flux density $\mathbf{B}$, is oriented transversely to the flowing plasma moving with a velocity $\mathbf{v}$. Electrically charged particles in the flowing combustion products, experience induced electromotive field $\mathbf{u} \times \mathbf{B}$ which results in an electric current collected by the electrodes. The electrodes are positioned on the opposite sides of the duct housing the flowing plasma.

The magnetic force on a moving particle, defined from the Lorentz force
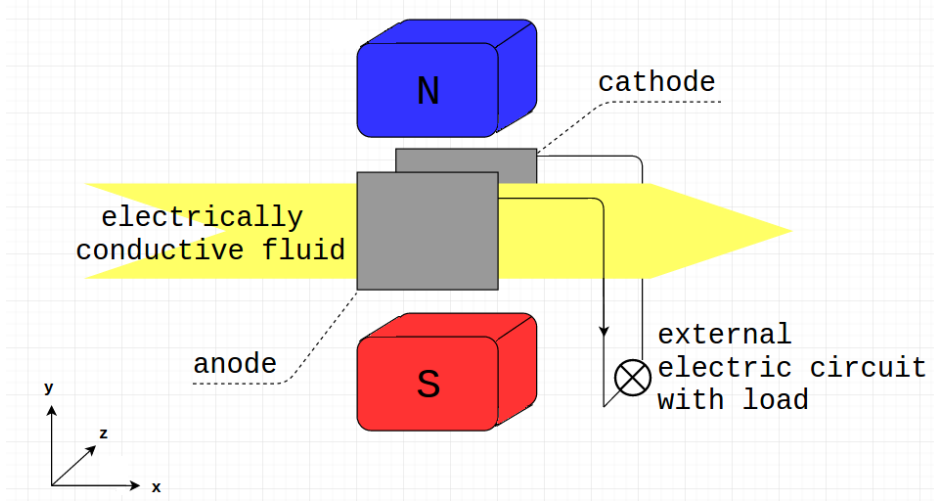
Figure 1.1: The underlying idea of MHD generator.

law is given by

$$\mathbf{F} = e\mathbf{v}_e \times \mathbf{B} \tag{1}$$

where the charge of a particle is e (ions and electrons), such that the particle experience a force $\mathbf{F}$ in a direction mutually perpendicular to the velocity vector $\mathbf{v}_e$ and magnetic the field vector $\mathbf{B}$ (Fig. 1.2). The current density can be written as

$$\mathbf{J} = -en_e\mathbf{v}_e \tag{2}$$

where n_e is electron concentration. The electron mobility is given by

$$\mu_e = \nu_e \frac{e}{m_e} \tag{3}$$

where ν_e the electron mean collision frequency and m_e is the electron mass. The electrical conductivity is described by

$$\sigma = \frac{e^2}{m_e\nu_e}n_e \tag{4}$$

Keeping in mind Eq. (2), (3) and (4) it is possible to obtain the equation describing the behaviour of electrically charged species caused by magnetic and electric fields, known as the generalized Ohm's law

$$\mathbf{J} = \sigma(\mathbf{E} + \mathbf{u} \times \mathbf{B}) - \mu_e\mathbf{J} \times \mathbf{B} \tag{5}$$
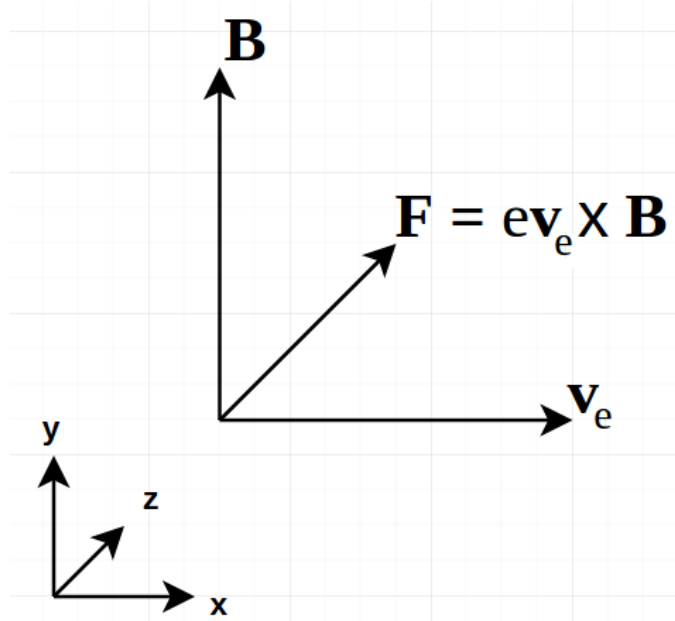
Figure 1.2: Elementary forces acting in MHD channel

where the element $\sigma(\mathbf{E}+\mathbf{u}\times\mathbf{B})$ represents the Faraday current while $\mu_e\mathbf{J}\times\mathbf{B}$ constitutes the Hall current. The former emerges from the net electromotive force in a conductive fluid while the latter is caused by the element $e\mathbf{v}_e \times \mathbf{B}$ which is the force acting on charged particles. The conduction force $\mathbf{J}$ is related with the electric field $\mathbf{E}$, generated by the potential difference between the electrodes.

The Lorentz force on the fluid is described by

$$\mathbf{F}_f = \mathbf{J} \times \mathbf{B} \tag{6}$$

and acts in a direction perpendicular to the plasma flow. Detailed layout of described vectors is presented in Fig. 1.3.

Considering that the power extracted from the gas by the Lorentz force per unit volume is given by

$$\mathbf{P}_f = \mathbf{u} \cdot \mathbf{F}_f \tag{7}$$

and that the electric power density delivered to the external load can be described as

$$\mathbf{P}_d = \mathbf{J} \cdot \mathbf{E} \tag{8}$$

the electrical efficiency of the MHD generator can be defined as

3

$$\eta_{el} = \frac{\mathbf{P}_d}{\mathbf{P}_d} \tag{9}$$

Typical values of the described parameters are given in Table 1.1 [2, 6]. The loading parameter is given by

$$K \equiv \frac{E_y}{uB} \tag{10}$$

while the plasma performance factor is defined as

$$ppf = \frac{JE}{B^2} \tag{11}$$

Table 1.1: Example values of MHD channel parameters

Property	Symbol	Indicative value	Unit
Magnetic flux density	$\mathbf{B}$	8	T
Electrical power density	$\mathbf{P}_d$	40	MW/m3
Flow velocity	v	1000	m/s
Plasma electrical conductivity	σ	20	S/m
Current density	J y	8000	A/m2
Loading parameter	K	0.8	-
The plasma performance factor	ppf	1.50E+006	W/m3 T2
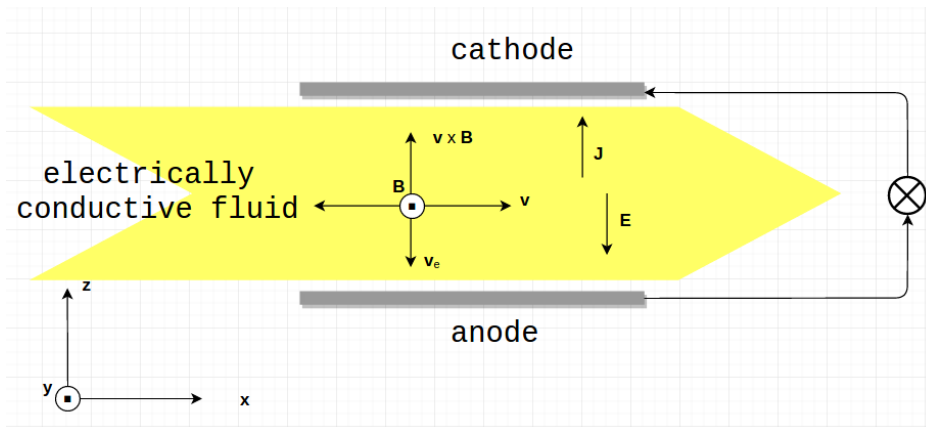
Figure 1.3: Vector and forces configuration inside the channel

The MHD generator can can be considered as an electromagnetic turbine. Unlike most of the heat engines the output energy in the magnetohydrodynamic generator is an electrical rather than mechanical energy. Since no

mechanically moving parts are involved, the MHD generator has a great thermodynamic advantage that the maximum working temperature is not limited by mechanical strength of materials but by the compatibility with high heat flux environments. As a result, the temperature of the working fluid is significantly higher than in the conventional Brayton based cycles, like a gas turbine. Today's gas turbines can withstand maximum temperatures in the range of 1700 K [3], while the upper temperature in MHD generator is constrained only by the plasma temperature which can be even 3600 K [2]. Because of that, magnetohydrodynamic generators are often considered as a topping cycle for conventional Brayton and Rankine cycles to increase general thermal efficiency and the idealised Carnot efficiency. Furthermore, the higher the temperature of a working fluid, the greater should be the value of its conductivity [4] which is the decisive aspect of the MHD practical, full-scale application in the future. Additionally, the absence of moving parts allows to reduce mechanical losses.

There are two fundamental types of MHD generators: open cycle generators where the working fluid (plasma) is produced in the combustion process and closed cycle involving internal gas heated in heat exchanger. We can also distinguish a case in which plasma is seeded in order to increase its electrical conductivity and unseeded configuration where working fluid is ionized only by chemical ionization.
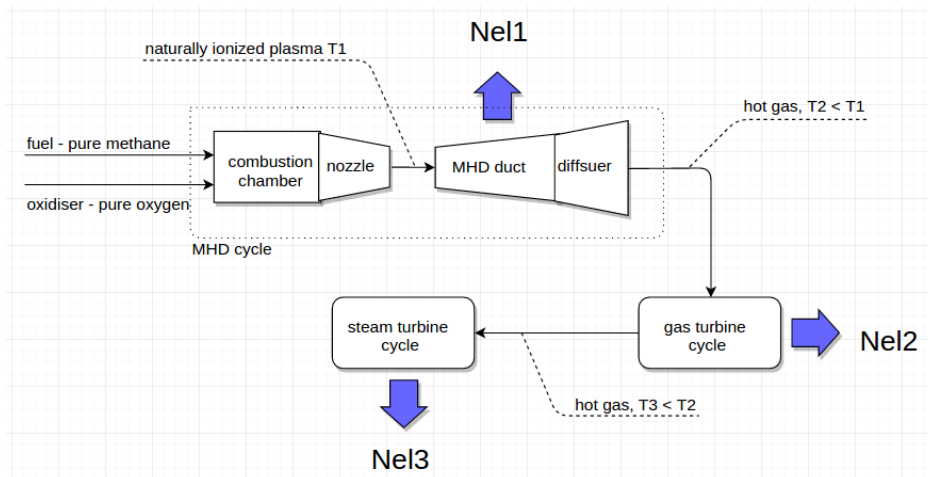
Figure 1.4: Block diagram of triple cycle power plant.

Many arrangements of power plants including MHD generators have been studied [2, 5, 6]. The heat can be supplied by combustion of fossil fuels such as coal, natural gas or specially prepared fuels like pure methane or hydrogen. Renewable sources of energy are also considered [2]. There are different

approaches in terms of how many thermodynamic cycles can be combined in the power plant. It should be emphasized that the temperature of the woking fluid in the outlet of the MHD channel is relatively high (about 1900 °C) [5]. It is therefore necessary to use that enthalpy in the next thermodynamic cycle. For this work, a triple cycle was proposed as a model case in which a MHD generator could be potentially utilized (Fig.1.4). In the work of Sufia et al. [5] it was shown that the overall efficiency of the triple cycle exceeds 70 %. The arrangement consist of an open, unseeded MHD channel, gas turbine and a steam turbine. Blue arrows (Fig. 1.4) indicate electric energy generated in each of the three modules of the power plant. The nozzle act as an element where working fluid is accelerated to a particular Mach number, while the diffuser makes it possible to convert the kinetic energy into pressure energy. The interaction between the electrically conductive plasma and a stationary magnetic field takes place in the MHD duct. It is equipped with electrodes that are positioned on the diverging walls.

As presented in Fig. 1.4, pure oxygen has been utilised in the combustion process to obtain high temperature which yields a plasma with high electric conductivity. The presented cycle constitutes therefore a basis for CCS oxy-combustion system since according to the simple global combustion reaction

$$CH_4 + 2O_2 \rightarrow CO_2 + 2H_2O \tag{12}$$
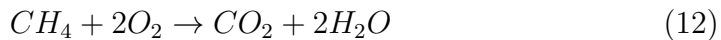
exhaust gases from the cycle should mainly contain water and carbon dioxide. Such a composition allows to implement relatively easy CO_2 capture method by means of water condensation.

The glory days of MHD development falls in the second half of 20th century. Advanced research and development programs were conducted in the United States and USSR in the 1970's and 1980's [2, 6]. One of the largest MHD power plant was built near Moscow [6]. This was a 25 MW combined heat and power - MHD power plant fired by natural gas. Another facility - 500 MW power plant - had been planned but its development was stopped by dissolution of the USSR and major technical problems (mainly insufficient plasma electrical conductivity which was the reason for inappropriately large magnet and channel size). The parameters characterizing the latter are presented in Table 1.2. In the US, Department of Energy conducted extensive work, including operating a 50MW magnetohydrodynamic power plant, fire by coal. Unfortunately, the whole development programme for MHD was stopped, mainly due to competition from the gas turbine combined cycle.

Summarizing, the MHD technology for generating electric energy was abandoned due to technical problems and a competition from more effective gas turbine combined cycles. As mentioned before - nowadays, in the light

Table 1.2: Basic parameters of gas fired, 500 MW USRR power plant

Parameter	U 500 USRR
total electric power [MW]	582
MHD cycle power [MW]	270
thermal efficiency [%]	53
temperature of combustion gas [K]	2900
temperature of preheated oxidizer [K]	1900
electrical conductivity [S/m]	9

of a stronger emphasis on carbon dioxide emission and CCS technology, the idea of MHD must be re-assessed. Additionally, the lack of seeding (implying regeneration and recycling) significantly simplifies the whole process and reduces greatly operating costs (those could represent as high as 20 % of costs of exploitation of the power plant [2]). There is, therefore, a great opportunity to combine CCS oxy-combustion technology with an MHD process resulting in high efficient carbon dioxide emission reduction and highly effective, combined cycle MHD power plant. Furthermore, since the last century, there is a significant technology development, a better understanding of plasma phenomena and a scientific progress.

1.2 Modification of GRI 3.0 combustion mechanism

1.2.1 Reactions and species

The combustion mechanism GRI - Mech 3.0 applied for the calculations includes 53 electrically neutral species and 325 reactions. In order to implement additional reactions that are taking electrons and ions into account (which is inevitable in calculating the electrical conductivity) modification was introduced. The changes were based on the document describing numerical simulation related with the effect of an electric field on flame stability [7]. As a result of the modification, two additional reactions with two extra species have been added

$$CH + O + H_2O \rightarrow CO + H_3O^+ + e^-$$ (13)

$$H_3O^+ + e^- \rightarrow H_2O + H$$ (14)
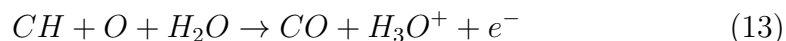
where e^- represents all the negative electrical species, i.e. electrons and anions. Such an assumption was possible since electrons are generally considered as the main negative charge carriers [7] .

For the case of positive electrical species, it is possible to say that the total amount of all the ions is practically equal to that of H_3O^+ [7]. Moreover, all ions have very similar transport coefficients. As a consequence of that, the term H_3O^+ appearing in Eq. 13 and Eq. 14 denotes all positive ions appearing in the reaction zone.

Eq.13 describes the chemical ionization reaction which rate is given by

$$k_{ionizaton} = 2.512 \times 10^{11} \times \exp\left(\frac{-7.118x10^3}{RT}\right)\left(\frac{cm^3}{mols}\right) \tag{15}$$

whereas Eq. 14 represents recombination reaction for electrically charged species with the rate of

$$k_{recombination} = 1.44 \times 10^{17}\left(\frac{cm^3}{mols}\right) \tag{16}$$

Eq. 15 and Eq. 16 are modified Arrhenius functions

$$k = AT^b \exp\left(\frac{-E}{RT}\right) \tag{17}$$

where k is the rate constant, A is the frequency factor, T is temperature, b is the Arrhenius constant, E is the activation energy and R is the gas constant.

It is important to underline that due to very small molar concentration of electrically charged particles, their impact on the chemistry of the 53 neutral species is negligible. An important corollary of that is the possibility of implementing Eq. 13 and Eq. 14 into GRI - Mech 3.0. Thermodynamic coefficients necessary to define H_3O^+ and e^- have been taken from the work of Bonnie et al. [8].

1.2.2 Electric conductivity

Implementation of the reactions described in the previous subsection provide the information about positive and negative charge fractions. However, to compare the results of calculations with other results available in the literature, it was necessary to calculate the electric conductivity of the obtained plasma which is given by

$$\sigma = \frac{e^2}{m\nu}n \tag{18}$$

where e is the elementary charge, n is the concentration of particles, m is the mass of particle and ν is the effective collision frequency. The values for electrons and positive ions used in the calculations are given in Table 1.3.

Effective collision frequencies rates have been calculated using values from the work of Itikawa [10].

Table 1.3: Values of factors for electrical charges

Particle	e [C]	m [kg]	ν [1/s]
e^-	1.602×10^{-19}	9.109×10^{-31}	4.179×10^{11}
H_3O^+	1.602×10^{-19}	3.159×10^{-26}	4.179×10^{11}

1.3 Results

For this work, a program have been written using the Python programming language with Cantera chemical kinetics package containing modified GRI - Mech 3.0 mechanism. The initial parameters of the simulations are presented in Table 1.4. A mixture of methane and oxygen is characterised by two states: non chemical equilibrium and chemical equilibrium. The process of equilibration have been conducted with constant pressure and enthalpy values. An ideal gas constant pressure reactor was applied. There are three cases of simulations with three different initial temperatures: 300 K, 1000 K and 1900 K. The latter value was chosen as the highest preheating temperature of air in MHD power plant that was found in the literature [6].

Table 1.4: Initial parameters

Property	Value	Unit
Mole fraction of CH_4	0.333	-
Mole fraction of O_2	0.667	-
Equivalence ratio	1	-
Pressure	1×10^5	Pa

The results from the calculations are presented in Table 1.5. Values of plasma electrical conductivity σ are highlighted as the most important parameter - that value is decisive in terms of the usage of non-seeded plasma in magnetohydrodynamic generators. T_b and T_a are the temperature of the mixture before and after equilibrium, X_{H3O+} and Y_{H3O+} are H_3O+ mole and mass fraction, whereas X_{e-} and Y_{e-} are electrons mole and mass fraction, respectively. n_e denotes electron concentration, σ_e is electrical conductivity of the mixture after equilibration, taking into account only electrons, σ_{H3O+}

Table 1.5: Calculated values for different cases

Symbol	Case A	Case B	Case C	Unit
T_b	300	1000	1900	K
T_a	3051	3125	3238	K
X_{H3O+}	7.41×10^{-9}	1.10×10^{-8}	1.88×10^{-8}	-
Y_{H3O+}	6.56×10^{-9}	1.01×10^{-8}	1.83×10^{-8}	-
X_{e-}	7.41×10^{-9}	1.10×10^{-8}	1.88×10^{-8}	-
Y_{e-}	1.88×10^{-13}	2.89×10^{-13}	5.25×10^{-13}	-
n_e	$1.76 \times 10^{+10}$	$2.55 \times 10^{+10}$	$4.20 \times 10^{+10}$	1/cm^3
n_e	3.45×10^{-10}	5.30×10^{-10}	9.63×10^{-10}	mole/g
σ_e	0.00119	0.00176	0.00300	S/m
σ_{H3O+}	3.42×10^{-8}	5.07×10^{-8}	8.66×10^{-8}	S/m
σ_{all}	0.00119	0.00176	0.00300	S/m

is electrical conductivity of the mixture after equilibration, taking into account only positive ions, σ_{all} is electrical conductivity of the mixture after equilibration. Additionally, the temperature and pressure impact on the electrical conductivity of the combustion gases was investigated. The results are presented in Fig.1.5.

1.4 Conclusions

The main goal of this work was to investigate the possibility of using a naturally ionized plasma as a working fluid in magnetohydrodynamic generators, without any additional seeding enhancing the electric conductivity.

It can be seen in Table 1.5 that the electric conductivity of the plasma varies with initial temperature of the mixture, however the great change in temperature (from 300 to 1900 K) causes only small variation of conductivity (the same order of magnitude). The value of 10^{-3} S/m is rather low - to obtain meaningful results in an MHD generator, electrical conductivity of plasma should range from 10 to 20 S/m [6, 11, 5] which is four orders of magnitude more than the values calculated in this work.

In order to check the correctness of the results, the literature has been surveyed to find a congruous measurements. A work of C.J. Harris et al. [11]. describes an experiment in which electrical conductivity of air produced in a shock tube were investigated - both seeded and unseeded. Despite the fact that the parameters and conditions during the described test are different than those in Cantera combustion calculations, the document constitutes a meaningful and important clue and helps to evaluate the calculations. In
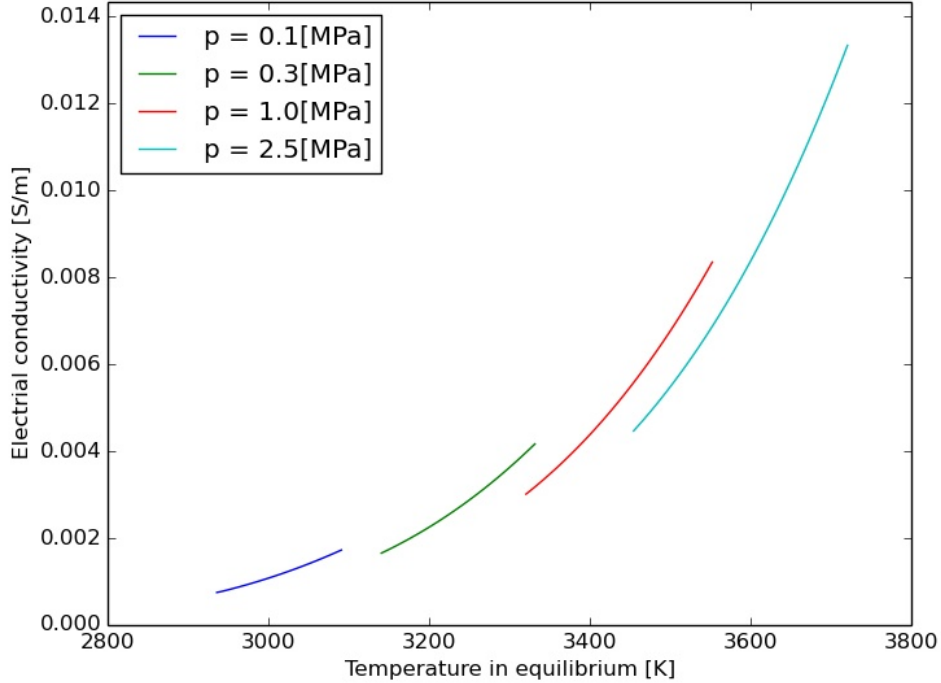
Figure 1.5: Electrical conductivity as a function of the temperature in equilibration for different values of initial pressure

the document it is possible can distinguish three cases: unseeded test flow of air in experiment 1, seeded air flow in experiment 1 and unseeded airflow in experiment 2 . Table 1.6 presents the comparison of selected parameters from the paper with values originating from the Cantera calculation whereas Fig.1.6 presents electron concentrations as a function of different temperatures, pressures and entropies [11].

Electron concentration (Table 1.6, light blue cells) in unseeded test section (T = 4000 K) and in Cantera calculations (T = 3051K) are very similar, as well as values of electrical conductivity. In both cases seeding was not included. As for the seeded air flow (I) (light yellow cells in the same table), electron concentration is higher compared with calculated values (and, in consequence, value of electrical conductivity is also higher) which should not be a surprise since additional seeding material increase electrical conductivity and electron charge concentration. Those are justifiable grounds for believing that conducted calculations may be correct. What is more, in the work of Harris et al. (1966) [11] only electrons were mentioned. That fact

Table 1.6: Comparison of Cantera results with values from the work of C.J.Harris et al.

Case	T, K	p, kPa	$n_e, 1/cm^3$	$n_e, mole/gram$	$\sigma_{all}, S/m$
A	3051	100	1.76×10^{10}	3.45×10^{-10}	0.00119
I	4000	1×10^5	-	1×10^{-10}	0.001
I	5300	122	1×10^{14}	-	20
II	7000	3000	-	-	150

where A is Cantera - case A, I denotes unseeded test section, II is Seeded air flow, III Unseeded Air flow.

confirms very low value of ions electrical conductivity compared to electron conductivity in Table 1.5. High electrical conductivity of unseeded air in the second experiment was due to extremely high temperatures which would be highly difficult to obtain in the industrial environment by means of oxy-fuel.

Conducted calculations and surveyed literature strongly suggests that the high temperature plasma bereft of additional seeding can not be used as an effective working fluid in the MHD channel. Reasonably attainable temperature in the oxy-combustion process does not provide an exhaust gases characterized by the sufficiently high electrical conductivity. Although the raise in temperature and pressure increase electrical conductivity, values of those parameters would have to exceed the level attainable in industrial environment.
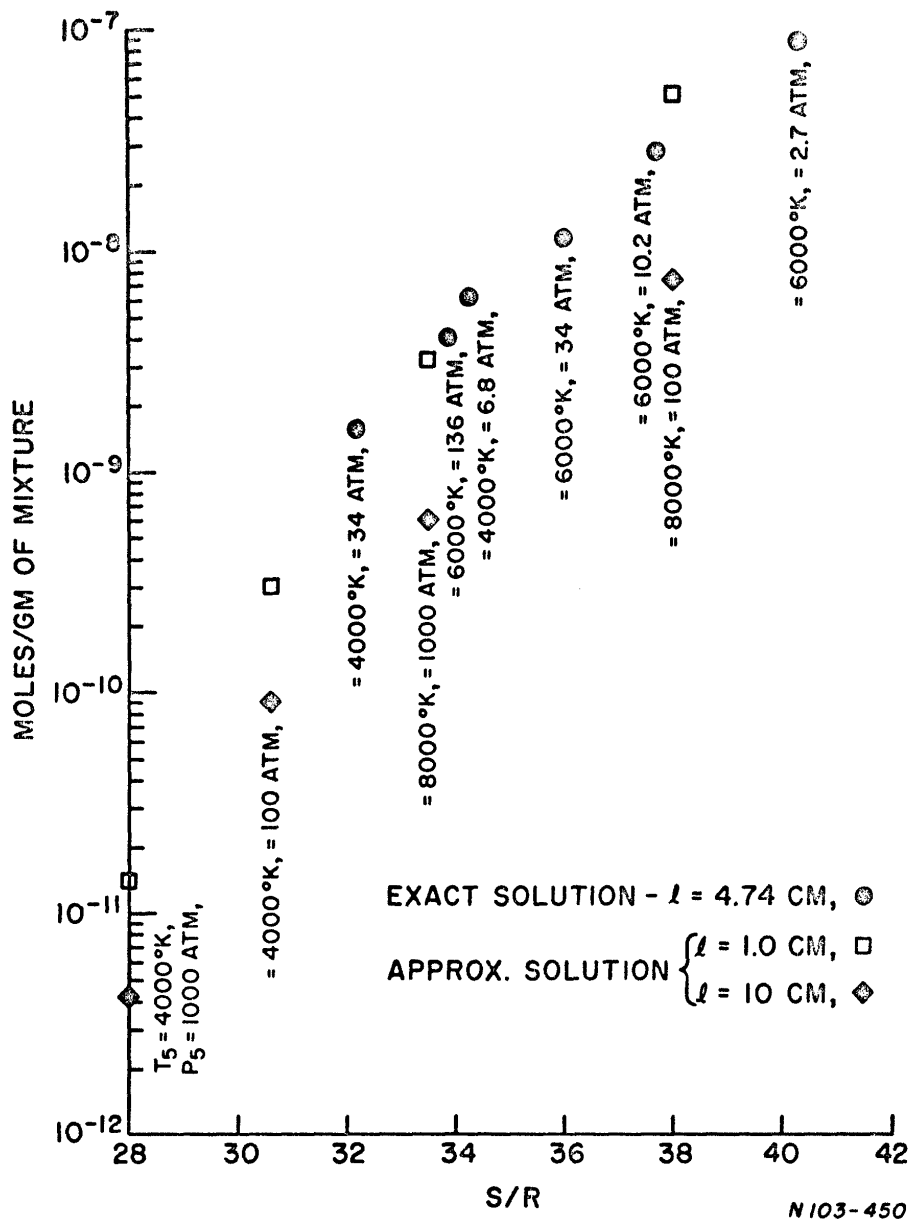
Figure 1.6: Different electron concentration for unseeded air test flow

13

2 Evaluation of chemiluminescence of excited species during combustion reaction

2.1 Theoretical framework

Chemiluminescence, as an electromagnetic emission of light, is produced by excited species coming back to the ground state. Molecule excitation results from a chemical process, where the excited species are produced through chemical reactions in the combustion zone. Eq. 19 presents the idea of de-excitation process, based on methylidyne radical. Excited species are customarily marked with an an asterisk.

$$CH^* \rightarrow CH + \gamma \tag{19}$$

where γ represents a photon of light. It is important to underline that excited species can get back to the ground state through collision reactions, called quenching reactions which do not involve the emission of light. Eq. 20 constitutes an example of a quenching reaction for excited CH, with N_2 as the collision partner:

$$CH^* + N_2 \leftrightarrow CH + N2. \tag{20}$$
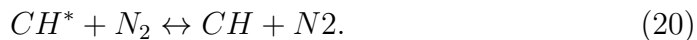
The chemiluminescence emission is weakly dependent on the combustion temperature but, on the other hand, strongly dependent on chemical composition [12]. In a hydrocarbon flame, which is the subject of this study, the highest intensities of the light emission in a specific spectrum is related with CH^* and OH^*. The emission of excited CH is apparent in three wavelength regions: near 314, 390 and 431 nm, while for excited OH the peak should be visible near 309 nm [12]. Another important sources of chemiluminescence are CO_2* around 415 [15] nm and C_2 near 510 nm [17].

Chemiluminescence plays an important role in oxy-fuel combustion. It provides useful data relating to diagnostic applications and flame sensing. Intensities of emission can provide informations about flame position, its structure and shape, allows to control fuel to air ratio and enables to measure heat release fluctuations [13]. Chemiluminescence has, therefore, an enormous potential for flame monitoring applications in the industrial environment.

2.2 Mechanism for the excited species

To evaluate measured values of excited species intensities, there was a need to implement Cantera package with relevant combustion mechanism. Standard GRI - Mech 3.0 does not include the reactions involving any excited species. It was, therefore, necessary to implement a suitable modification of the combustion mechanism. In the first stage, two sets of reactions for two types of flames had been examined from the work of De Leo et al. (207) [12] - describing diffusion flame and from the paper of Nori et al. (2008) [14] - describing premixed flame. Mechanisms are presented in Table 2.1 and Table 2.2. There are differences between those two sets of reactions, including coefficient values, number of reactions and amount of species. Many different configurations has been tested to choose the most accurate one for the further calculations. As a conclusion, mechanism from the paper of Nori et al. (2008) has been chosen, however with a modification.

One of the intriguing differences between the two mechanisms is a type of the OH* removal reactions. It is possible to notice that for the premixed flame (Reactions Q1 - Q10 in Table 2.2) forward reactions had been chosen, whereas for diffusion flame (Reactions R3 - R9 in Table 2.1), for the same set, reversible reactions had been adopted. There is no such a difference for excited CH, thus the impact of the reaction type (reversible and forward) was investigated for CH*. As a model example, to have a possibility to compare the results with a reliable data, charts from the work of Maurizio et al. had been chosen (Fig. 2.1). Then, calculations, similar to those presented in the work of De Leo et al. [12] were conducted for the diffusion flame. In the first case, all the removal reactions were reversible (as originally in Table 2.2)) and in the latter, the reactions were changed for forward reactions. Results are presented in fig. 2.2. The conclusions are as follows:

The temperature distribution along the position of the flame for both cases is practically the same as in the model example. It should not be surprising since the concentration of excited species is generally over a dozen orders of magnitude lower than the concentration of chemical compounds in a ground state - the temperature is therefore not affected by the change of the reaction type for excited CH. Distribution of OH and CH in a ground state is similar to the distribution presented in the paper. There are, therefore differences in concentration of those species in the excited state. It can be noted that concentration of OH* in case a and b is of the same order of magnitude as in model case. The concentration of CH*, however, differs significantly - in case a - with reversible quenching reactions (original model from Table 2.2) CH in the excited state is 5 orders of magnitude higher then in the case b - with forward reactions. The crucial conclusion is that the

Table 2.1: Combustion mechanism for diffusion flame

#	Reaction	A	n	E
R1	$O + H + M \Leftrightarrow OH^* + M$	1.2×10^{13}	0	6940
		3.63×10^{13}	0	0
		6.0×10^{14}	0	6940
R2	$CH + O_2 \Leftrightarrow CO + OH^*$	3.72×10^{10}	0	167.2
		4.8×10^{10}	0	0
		6.0×10^{10}	0	0
		1.8×10^{11}	0	0
		4.0×10^{13}	0	0
		4.8×10^{13}	0	0
R3	$OH^* + N_2 \Leftrightarrow OH + N_2$	1.08×10^{11}	0.5	-1238
R4	$OH^* + O_2 \Leftrightarrow OH + O_2$	2.10×10^{12}	0.5	-482
R5	$OH^* + H_2O \Leftrightarrow OH + H_2O$	5.92×10^{12}	0.5	-861
R6	$OH^* + H_2 \Leftrightarrow OH + H_2$	2.95×10^{12}	0.5	-444
R7	$OH^* + CO_2 \Leftrightarrow OH + CO_2$	2.75×10^{12}	0.5	-968
R8	$OH^* + CO \Leftrightarrow OH + CO$	3.23×10^{12}	0.5	-787
R9	$OH^* + CH_4 \Leftrightarrow OH + CH_4$	3.36×10^{12}	0.5	-635
R10	$OH^* \Rightarrow OH$	1.45×10^{6}	0	0
		1.39×10^{6}	0	0
R11	$C_2 + OH \Leftrightarrow CO + CH^*$	1.1×10^{13}	0	0
R12	$C_2H + O \Leftrightarrow CO + CH^*$	$2.5(\pm0.8) \times 10^{12}$	0	0
		6.2×10^{12}	0	0
		1.08×10^{13}	0	0
R13	$C + H + M \Leftrightarrow CH^* + M$	3.63×10^{13}	0	0
R14	$C_2H + O_2 \Rightarrow CO_2 + CH^*$	2.17×10^{10}	0	0
		$3.2(\pm1.0) \times 10^{11}$	0	805
		2.5×10^{12}	0	0
		4.1×10^{13}	0	4500
		4.5×10^{15}	0	25000
R15	$CH^* \Rightarrow CH$	1.86×10^{6}	0	0
		2.1×10^{6}	0	0
		2.08×10^{6}	0	0
		2.25×10^{6}	0	0
		2.17×10^{6}	0	0
		1.87×10^{6}	0	0
		1.97×10^{6}	0	0
		2.27×10^{6}	0	0
R16	$CH^* + N_2 \Leftrightarrow CH + N_2$	3.03×10^{2}	3.4	-381
R17	$CH^* + O_2 \Leftrightarrow CH + O_2$	2.48×10^{6}	2.14	-1720
R18	$CH^* + H_2O \Leftrightarrow CH + H_2O$	5.3×10^{13}	0	0
R19	$CH^* + H_2 \Leftrightarrow CH + H_2$	1.47×10^{14}	0	1361
R20	$CH^* + CO_2 \Leftrightarrow CH + CO_2$	0.241	4.3	-1694
R21	$CH^* + CO \Leftrightarrow CH + CO$	2.44×10^{12}	0.5	0
R22	$CH^* + CH_4 \Leftrightarrow CH + CH_4$	1.73×10^{13}	0	167
R23	$C_2 + H_2 \Leftrightarrow C_2H + H$	4×10^{5}	2.4	1000
R24	$CH + CH \Leftrightarrow C_2 + H_2$	5×10^{12}	0	0
R25	$C + C + M \Leftrightarrow C_2 + M$	3×10^{14}	0	0
R26	$C + CH \Leftrightarrow C_2 + H$	5×10^{13}	0	-1000
R27	$O + C_2 \Leftrightarrow C + CO$	5×10^{13}	0	0
R28	$C_2 + O_2 \Leftrightarrow CO + CO$	9×10^{12}	0	980

[a] Reaction rate coefficients given in the form $k = AT^b \exp(-E/RT)$. Units are mol cm cal s.

Table 2.2: Combustion mechanism for premixed flame

#	Reaction	A	b	E_a(cal)
R1	$H + O + M \leftrightarrow OH^* + M$	6×10^{14}	0.0	6940
R3	$CH + O_2 \leftrightarrow OH^* + CO$	3.24×10^{14}	-0.4	4150
Q1	$OH^* + H_2O \rightarrow OH + H_2O$	5.92×10^{12}	0.5	-861
Q2	$OH^* + CO_2 \rightarrow OH + CO_2$	2.75×10^{12}	0.5	-968
Q3	$OH^* + CO \rightarrow OH + CO$	3.23×10^{12}	0.5	-787
Q4	$OH^* + H_2 \rightarrow OH + H_2$	2.95×10^{12}	0.5	-444
Q5	$OH^* + O_2 \rightarrow OH + O_2$	2.10×10^{12}	0.5	-482
Q6	$OH^* + OH \rightarrow OH + OH$	1.50×10^{12}	0.5	0.0
Q7	$OH^* + H \rightarrow OH + H$	1.50×10^{12}	0.5	0.0
Q8	$OH^* + O \rightarrow OH + O$	1.50×10^{12}	0.5	0.0
Q9	$OH^* + N_2 \rightarrow OH + N_2$	1.08×10^{11}	0.5	-1238
Q10	$OH^* + CH_4 \rightarrow OH + CH_4$	3.36×10^{12}	0.5	-635
R6	$C_2H + O \leftrightarrow CH^* + CO$	6.023×10^{12}	0.0	457
R7	$C_2H + O_2 \leftrightarrow CH^* + CO_2$	6.023×10^{-4}	4.4	-2285.1
Q1	$CH^* + H_2O \leftrightarrow CH + H_2O$	5.3×10^{13}	0.0	0.0
Q2	$CH^* + CO_2 \leftrightarrow CH + CO_2$	2.41×10^{-1}	4.3	-1694
Q3	$CH^* + CO \leftrightarrow CH + CO$	2.44×10^{12}	0.5	0.0
Q4	$CH^* + H_2 \leftrightarrow CH + H_2$	1.47×10^{14}	0.0	1361
Q5	$CH^* + O_2 \leftrightarrow CH + O_2$	2.48×10^{6}	2.14	-1720
Q6	$CH^* + N_2 \leftrightarrow CH + N_2$	3.03×10^{2}	3.4	-381
Q7	$CH^* + CH_4 \rightarrow CH + CH_4$	1.73×10^{13}	0.0	167

case b (Fig. 2.2) is consistent with the model case from the reference paper (Fig. 2.1). For that reason, in the further calculations, the model from the work of Nori et al. was modified by changing the type of reactions Q1 to Q2 (from Table 2.2) from reversible to forward. Such a correction allowed for higher accuracy in the measurements verification. Finally, the set of reactions describing excited CO_2^* was implemented from the work of Kopp et al. [15] The full mechanism used for calculations is presented in Table 2.3.
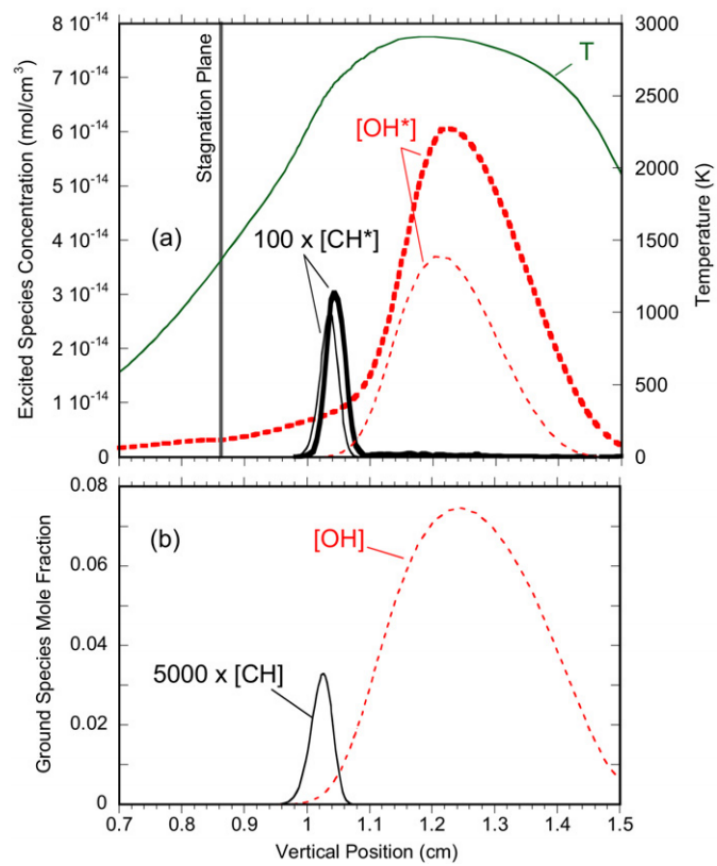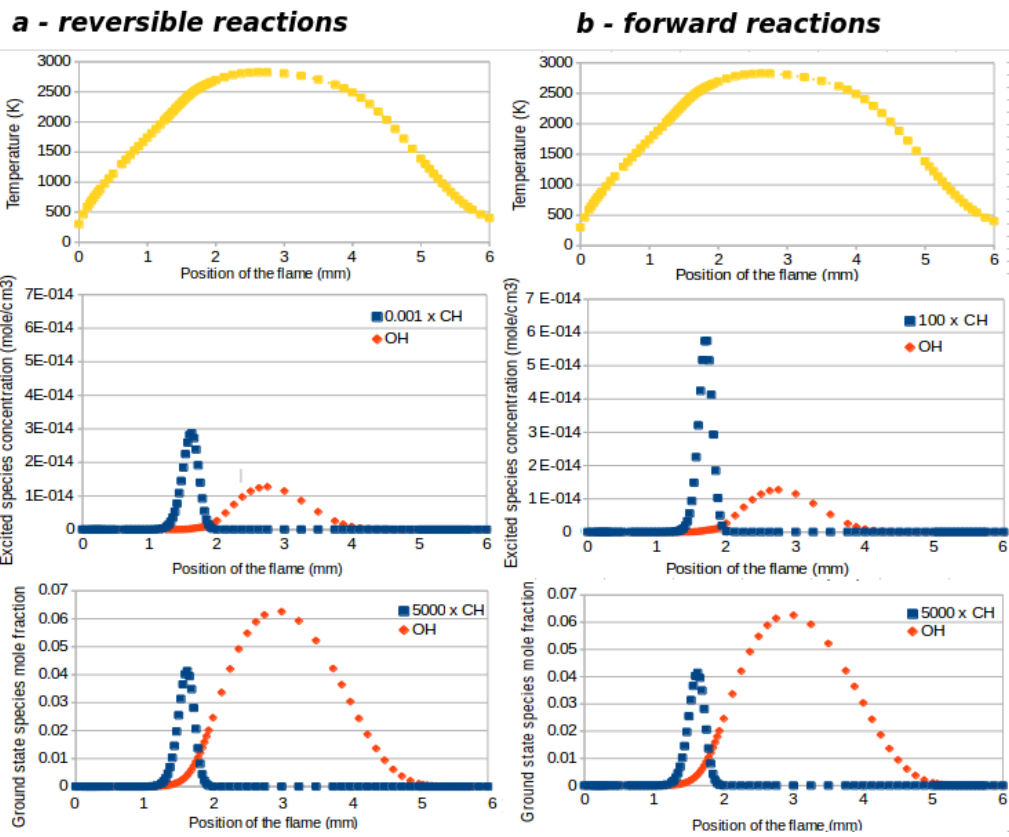
Figure 2.1: Reference paper model

Figure 2.2: Comparison of results from two mechanism with different reaction type for excited CH

Table 2.3: Combined combustion mechanism for CH* OH* and CO_2*

#	Reaction	A	b	$E_a(cal)$	Ref.
R326	H + O + M $\leftrightarrow$ OH* + M	6×10^{14}	0.0	6940	[14]
R327	CH + O$_2$ $\leftrightarrow$ OH* + CO	3.24×10^{14}	-0.4	4150	[14]
R328	OH* + H$_2$O $\rightarrow$ OH + H$_2$O	5.92×10^{12}	0.5	-861	[14]
R329	OH* + CO$_2$ $\rightarrow$ OH + CO$_2$	2.75×10^{12}	0.5	-968	[14]
R330	OH* + CO $\rightarrow$ OH + CO	3.23×10^{12}	0.5	-787	[14]
R331	OH* + H$_2$ $\rightarrow$ OH + H$_2$	2.95×10^{12}	0.5	-444	[14]
R332	OH* + O$_2$ $\rightarrow$ OH + O$_2$	2.10×10^{12}	0.5	-482	[14]
R333	OH* + OH $\rightarrow$ OH + OH	1.50×10^{12}	0.5	0	[14]
R334	OH* + H $\rightarrow$ OH + H	1.50×10^{12}	0.5	0	[14]
R335	OH* + O $\rightarrow$ OH + O	1.50×10^{12}	0.5	0	[14]
R336	OH* + N$_2$ $\rightarrow$ OH + N$_2$	1.08×10^{11}	0.5	-1238	[14]
R337	OH* + CH$_4$ $\rightarrow$ OH + CH$_4$	3.36×10^{12}	0.5	-635	[14]
R338	OH* $\rightarrow$ OH + γ	1.85×10^{6}	0.0	0	[14, 12]
R339	C$_2$H + O $\leftrightarrow$ CH* + CO	6.023×10^{12}	0.0	457	[14]
R340	C$_2$H + O$_2$ $\leftrightarrow$ CH* + CO$_2$	6.023×10^{12}	4.4	-2285	[14]
R341	CH* + H$_2$O $\rightarrow$ CH + CH$_4$	5.3×10^{13}	0.0	0	[14]
R342	CH* + CO$_2$ $\rightarrow$ CH + CO$_2$	2.75×10^{-1}	4.3	-1694	[14]
R343	CH* + CO $\rightarrow$ CH + CO	3.23×10^{12}	0.5	0	[14]
R344	CH* + H$_2$ $\rightarrow$ CH + H$_2$	2.95×10^{14}	0.0	1361	[14]
R345	CH* + O$_2$ $\rightarrow$ CH + O$_2$	2.10×10^{6}	2.1	-1720	[14]
R346	CH* + N$_2$ $\rightarrow$ CH + N$_2$	1.08×10^{2}	3.4	-381	[14]
R347	CH* + CH$_4$ $\rightarrow$ CH + CH$_4$	3.36×10^{13}	0.0	167	[14]
R348	CH* $\rightarrow$ CH + γ	1.4×10^{6}	0.0	0	[14]
R349	CO + O + M $\leftrightarrow$ CO_2* + M	4.00×10^{14}	0.0	2384	[15]
R350	HCO + O $\leftrightarrow$ CO_2* + H	3.00×10^{13}	0.0	0	[15]
R351	CO$_2$* + Ar $\rightarrow$ CO$_2$ + Ar	8.42×10^{12}	0.5	0	[15]
R352	CO$_2$* + H$_2$O $\rightarrow$ CO$_2$ + H$_2$O	8.34×10^{12}	0.5	0	[15]
R353	CO$_2$* + CO$_2$ $\rightarrow$ CO$_2$ + CO$_2$	9.12×10^{12}	0.5	0	[15]
R354	CO$_2$* + CO $\rightarrow$ CO$_2$ + CO	9.69×10^{12}	0.5	0	[15]
R355	CO$_2$* + H $\rightarrow$ CO$_2$ + H	3.07×10^{13}	0.5	0	[15]
R356	CO$_2$* + H$_2$ $\rightarrow$ CO$_2$ + H$_2$	2.27×10^{13}	0.5	0	[15]
R357	CO$_2$* + O$_2$ $\rightarrow$ CO$_2$ + O$_2$	8.77×10^{12}	0.5	0	[15]
R358	CO$_2$* + O $\rightarrow$ CO$_2$ + O	9.82×10^{12}	0.5	0	[15]
R359	CO$_2$* + OH $\rightarrow$ CO$_2$ + OH	9.87×10^{12}	0.5	0	[15]
R360	CO$_2$* + CH$_4$ $\rightarrow$ CO$_2$ + CH$_4$	1.19×10^{13}	0.5	0	[15]
R361	CO$_2$* + N$_2$ $\rightarrow$ CO$_2$ + N$_2$	9.96×10^{12}	0.5	0	[15]
R362	CO$_2$* $\rightarrow$ CO$_2$ + γ	1.00×10^{6}	0.0	0	[15]

2.3   Measurements

For the sake of the chemiluminescence measurement, test rig has been constructed (Fig. 2.3 and Fig. 2.4). The experimental setup comprises two main sections: first part contain the burner with the control apparatus while the second one consists of a ICCD camera with an optical spectrometer and control unit (PC).
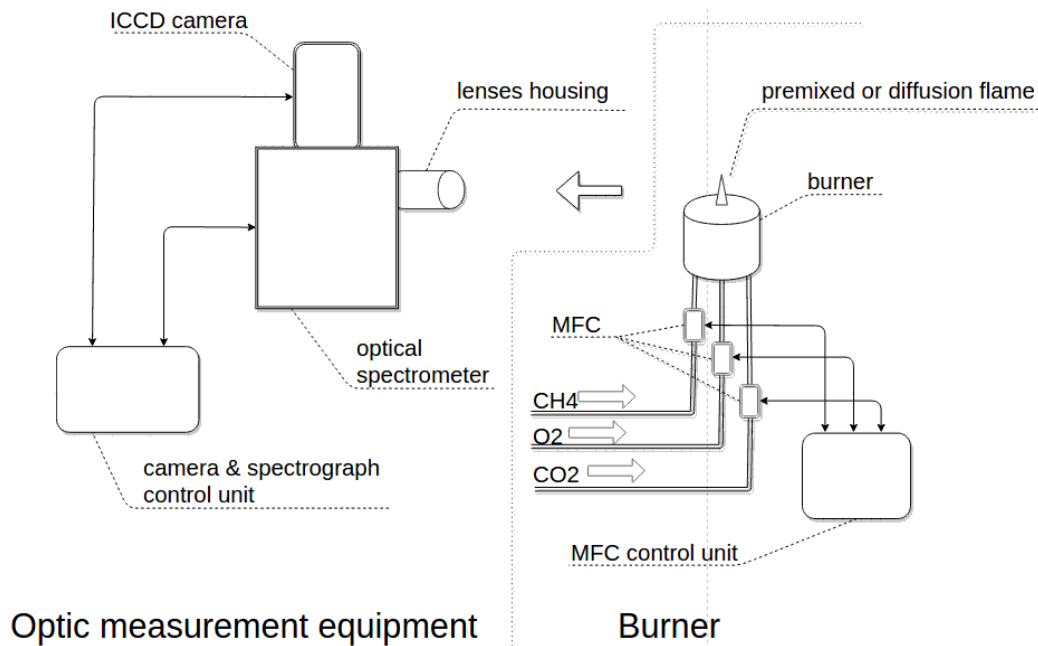
Figure 2.3: Experimental setup diagram

The process of combustion involved premixed, laminar flame with methane as a fuel. Oxidizer was a mixture of oxygen and carbon dioxide. For regulatory purposes, mass flow controllers (MFC) were applied. Additionally, the installation was equipped with safety valves connected with push button emergency stop.

During the experimental procedure, two burner types were applied - for laminar and premixed flame. The first one consisted of 2 mm tube delivering fuel flow inside the 69 mm pipe for oxidizer mixture. Additionally, to avoid unpredictable air drafts in the laboratory which could affect stability of the flame, a quartz tube was installed. Usage of quartz was adequate since that material is transparent for the whole wavelength range surveyed during the test process. For the premixed flame, the installation was constructed in such a manner that the mixing process was occurring in the piping system. That solution enabled to obtain the mixture of fuel and oxidiser before the burner
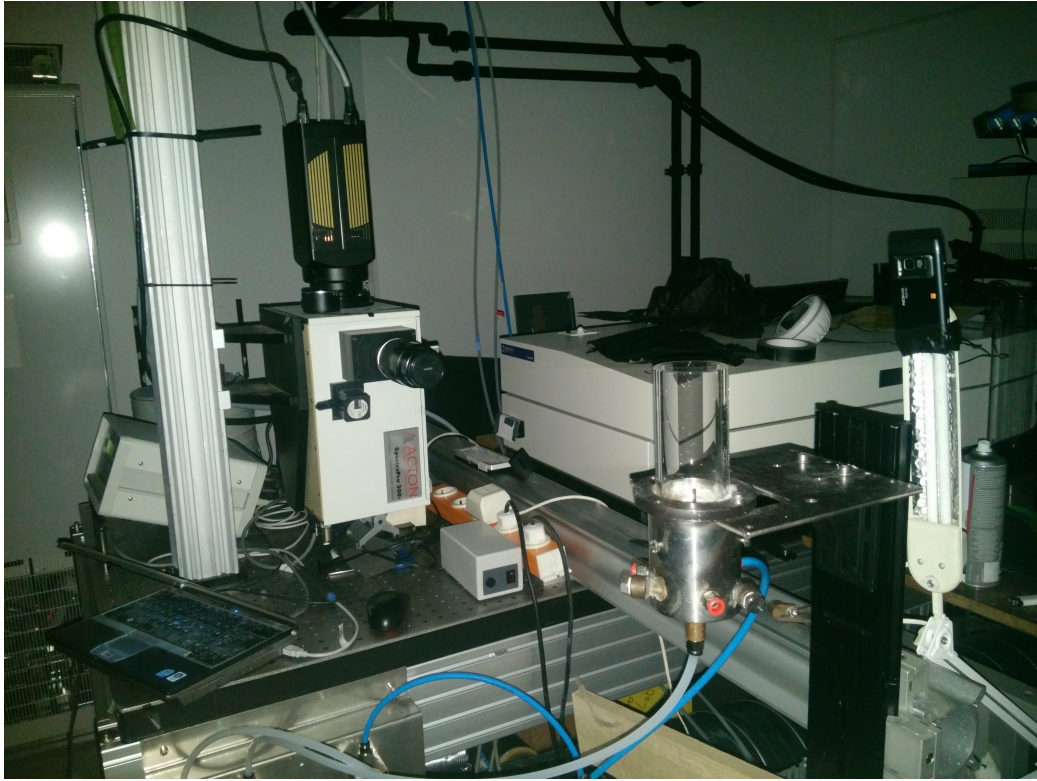
Figure 2.4: Photograph of the test rig

itself and avoid imperfect mixing inside the cylinder. For safety reasons, the burner was filled with glass spheres that serve as flame arrestor in case of flame flashback. Both burners have been placed in such a manner that the flame was situated 40 cm in front of camera objective.

Excited species emit electromagnetic radiation within a certain spectrum. To detect that spectrum, it was necessary to measure properties of the light emitted by the flame. The radiation path from a combustion zone to the camera sensor is presented in Fig. 2.5. First, the light coming from a flame is focused on the entrance slit of the optical spectrometer by a 105 mm UV lens. The opening of the slit could be regulated to define the amount of light entering the spectrometer. Then, the signal goes trough the set of mirrors with grating as a key element. The grating disperses emitted radiation according to its wavelength. In other words, the light is sorted by its wavelength. That enables to measure the intensity of radiation for a given spectrum and measure excited species intensities. Intensified CCD camera, used for the experiment was designed for macro and microscopy imaging in low light measurement. It was equipped with an image intensifier connected

to CCD array via optical fibers. The camera was characterized by several parameters: gate width defined a time in which camera sensor accumulated a signal from the flame, number of gates per exposure determined amount of images taken for one exposure, while gain defined intensification level. Parameters characterizing the camera, spectrograph and lens are listed in Table 2.4.
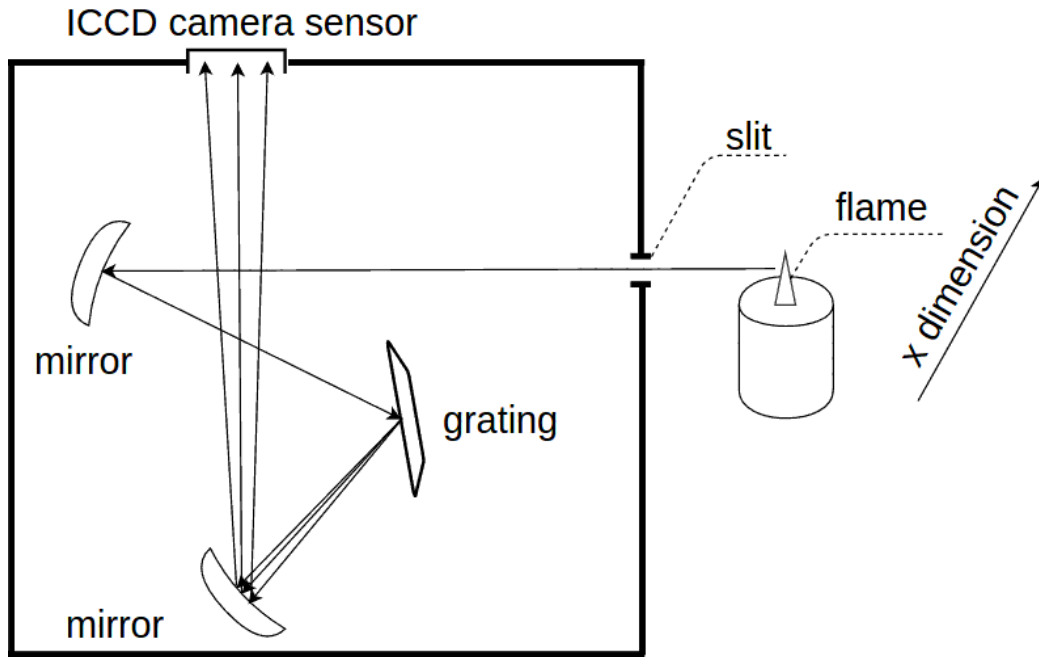
Figure 2.5: Optical path

Table 2.4: Lens, spectrometer and camera parameters

Parameter	Value	Unit
Slit opening	150	μm
Aperture	f/4.5	-
Gate width	700	us
Gates per exposure	40	-
Gain	115* 50**	-

Note: * for diffusion flame; ** for premixed flame

During the measurement process, photographies of studied flames were taken. Fig. 2.6 explains the process of an image creation. As an example, premixed flame were chosen but the idea is the same for the diffusion one.

Upper part of the Fig. 2.6 presents the ideal shape of the premixed flame from two different perspectives, while lower part shows a raw image resulting from the measurement procedure. Vertical dimension of the image represents wavelength, horizontal shows physical dimension (along the horizontal edge of the slit), while the colour of the pixels indicate intensity value. Red, vertical, dotted lines indicate the areas of the highest intensity values along the physical x dimension. The strongest signal occurring in those zones corresponds to the edges of the flame, from the camera perspective. Those areas were used for a further plotting of an intensity charts as a function of the wavelength. In order to obtain clear results, it was indispensable to prepare post-processing procedure for which the raw image was converted to ASCII file containing full set of informations. For that purpose, python programming language was implemented again. That solution made also possible to compile measurements with suitable Cantera script describing selected issues.
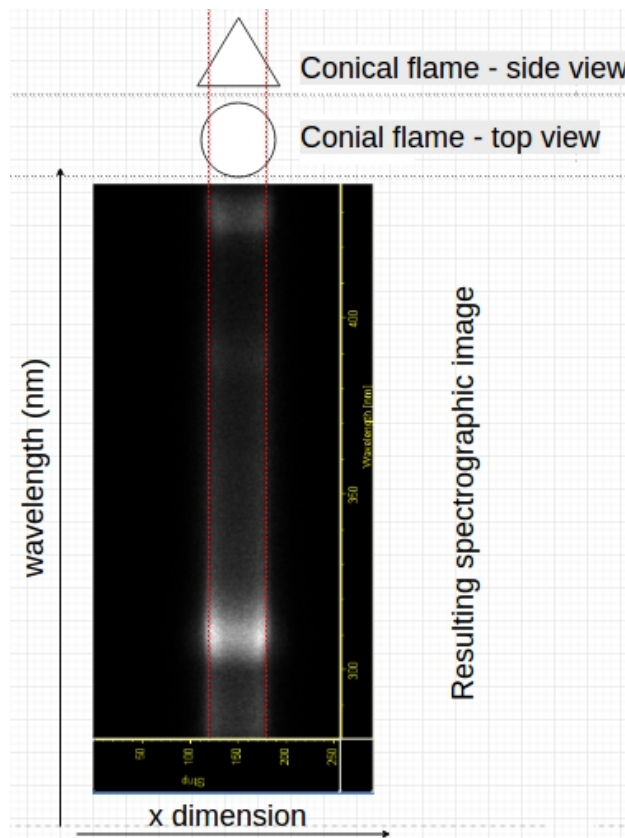
Figure 2.6: Sample image resulting from measurements

The whole detection system was calibrated against 2 lamps in order to

cover the full investigated spectrum. First lamp covered the range from 250 to 355 nm (ultraviolet range) while the second one from 350 to 550 nm (mostly the visible range). The procedure was implemented in Python post-processing script.

2.4 Results

Since Cantera constitutes an package for python programming language, it was possible to combine the calculations with post-processing script and create one consistent, easy-to-use and efficient programme. For the purpose of the calculations, two scripts for one dimensional calculations were implemented and modified: first one describing premixed, freely-propagating flame, whereas the latter depicted opposed, diffusion combustion precess. Fig. 2.7 presents connections between different modules in the post-processing script for the chemiluminescence measurements.
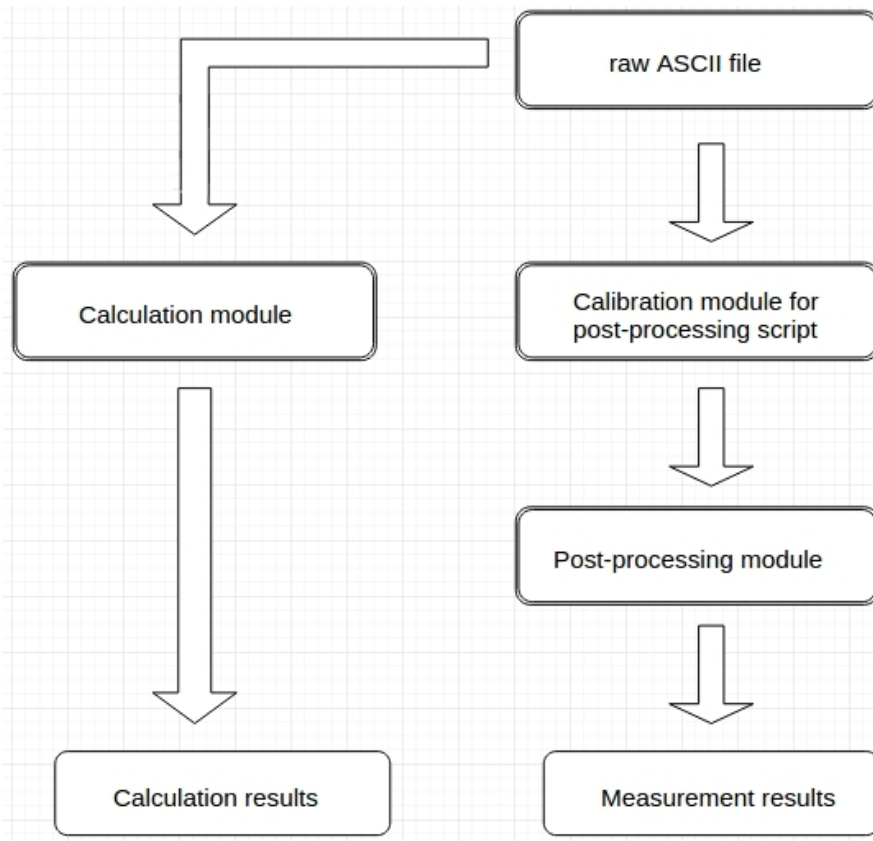
Figure 2.7: Flowchart describing post-processing system

2.4.1 Premixed flame

In the first stage of measurement procedure, premixed flame was investigated. As a fuel, methane was applied, whereas as an oxidizer, oxygen diluted in nitrogen or carbon dioxide was adopted. The flame was investigated for different oxygen content in the oxidizer, with constant equivalence ratios equal to one. Fig. 2.8 presents a photography, taken with the flash lamp to reveal the visual aspect of the flame. The reaction front is well visible in the bottom of the flame as a conical shape, followed by diffusion part of the flame.
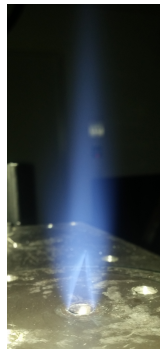
Figure 2.8: Premixed flame
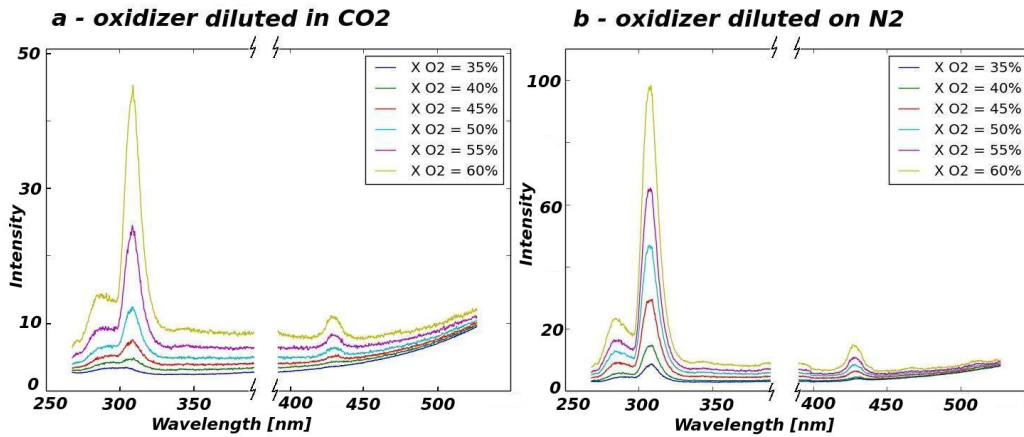
Figure 2.9: Intensity distribution for premixed flame

Fig. 2.9 presents light intensity as a function of wavelength. Top-left corner describes the lines in terms of oxygen content. Generally, intensity value represents the signal strength and has no unit. To have the possibility to

26
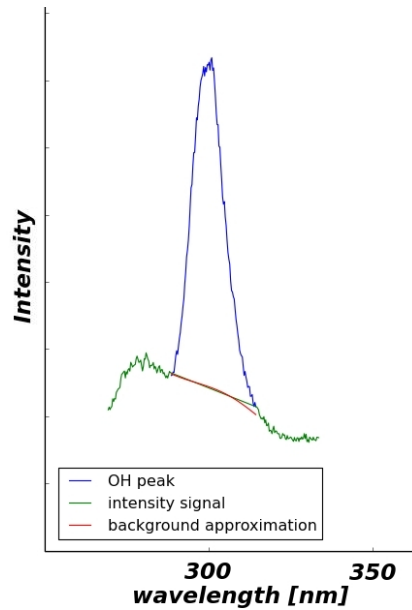
Figure 2.10: Background removal

compare the results, for different oxidizer diluent, the same camera parameters were chosen. The strongest electromagnetic intensity of methylidyne radical CH* is slightly shifted towards the central axis of the flame in relation to the OH* signal. Because of that two different regions from the ASCII file (image) were used for plotting (left side for OH* signal, right side for CH* and CO_2*). Empty spaces in the middle of the charts indicate those to regions. Two peaks of intensity are noticeable - excited OH signal occurs at 308 nm while CH* indicates its position at 431 nm. For each value of oxygen content in the oxidizer, the signal coming from excited species was calculated by integration for a given wavelength - for OH* between 301 and 322 nm , for CH* between 423 and 440 nm and additionally for CO_2* between 410 and 420 nm. Since CH* and OH* occured as an intensity peaks, the background coming from another sources of radiation had to be removed. Fig. 2.10 presents the methodology for its removal. The background was calculated as a sixth polynomial trend line, based on the intensity values for a wavelengths lower and higher than those corresponding to the peak. Emission of light coming from excited CO_2 was a part of the background so the procedure could not be applied. The results were plotted in Fig. 2.11. Because the measurements for both diluents were conducted for the same camera parameters, it was possible to normalize all the values, both measured and calculated and then compare the results.

Unquestionably, excited OH signal was the strongest among all three

investigated species, reaching the highest value for 60 % of oxygen diluted
in nitrogen. Generally, the raise in oxygen content (and, consequently, the
temperature rise) increases the emission of photons from the excited species.
Other studies [14, 12] confirms that trend. It is also possible to notice that
the emission of light coming from excited OH and CH is generally stronger
for the flame with nitrogen as a diluent in the oxidizer, especially for higher
values of oxygen content. CO_2* signals for different diluents are more similar.
In case of measurements, for N_2 as an oxidizer, the raise of excited carbon
dioxide signal is smooth while for OH* and CH* the slope is more visible. For
OH* and CH* calculations agree with measurements quite exactly, however
for CO_2* there is a discrepancy for lower values of oxygen content. In other
words, calculated CO_2* signal is more steep than measured one.
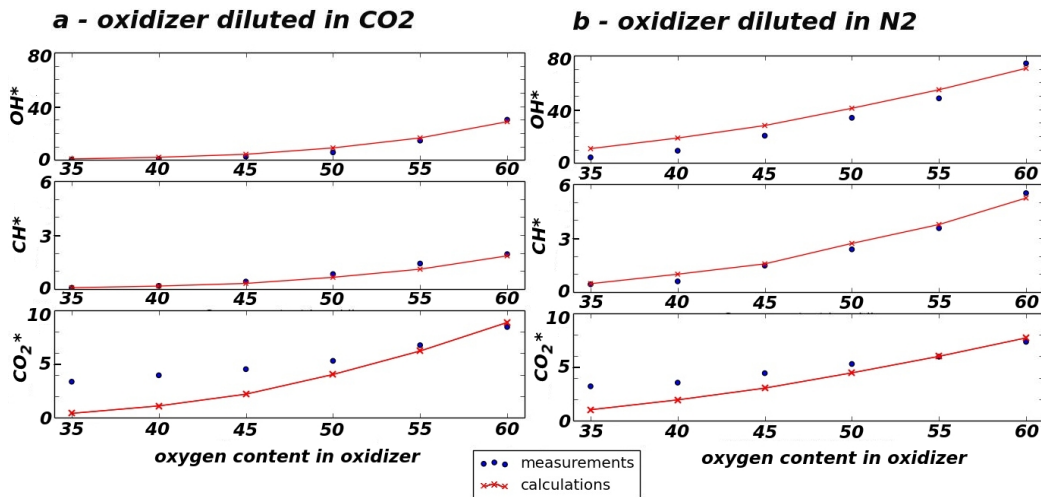
Figure 2.11: Excited species signal in the premixed flame

2.4.2 Diffusion flame

In the second stage of the experiment, diffusion flame was investigated. Fig.
2.12 presents photographies of the studied flame for different O_2 content in
the oxidizer. For high oxygen concentration - both with nitrogen and carbon
dioxide as a diluent, the flame is lower and more intense than in case of higher
dilution of the oxidizer. Moreover, the color of the flame indicates, that the
temperature raises as more oxygen per volume take part in the reaction zone.
It was also possible to notice that oxy-combustion flame is more stable.

For low O_2 content, there is a significant distinction in the flame with
different diluent - for 30 percent of oxygen, the base of the flame has a blue
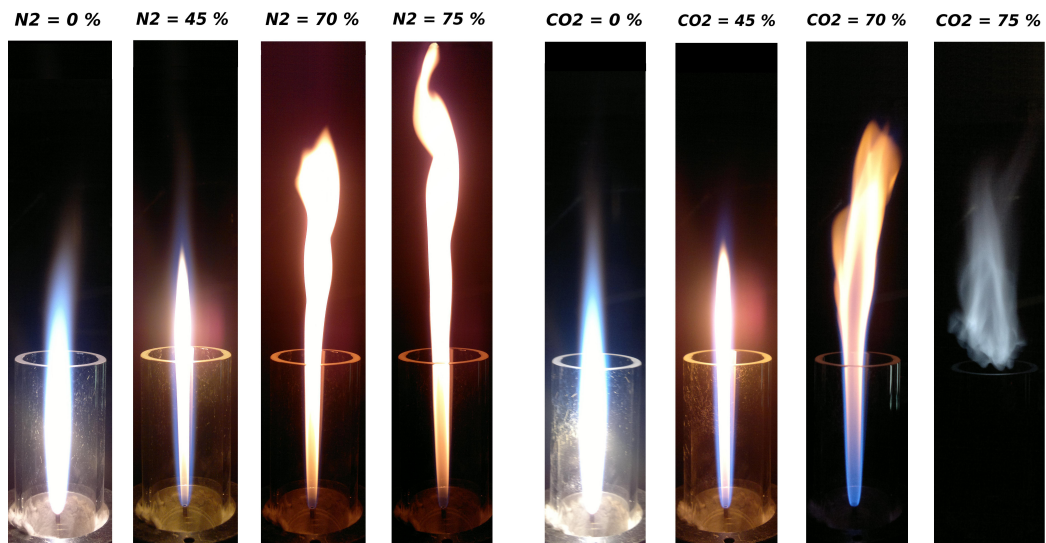
Figure 2.12: Visual comparison of diffusion flame for different oxygen content in the oxidizer with different diluent

hue (CO_2) while for N_2 it's orange. Furthermore, for $CO_2 = 75\%$, the flame is clearly raised and nearly blown out. Those symptoms are related to the fact that carbon dioxide has a higher value of heat capacity than nitrogen and CO_2 gains more heat from the reaction zone that nitrogen.

For diffusion flame, the same set of measurements were carried out. There were, however some crucial differences. In diffusion flames, soot formation is more prominent than in premixed flames, and a strong broadband emission disturbs the signal of species CH* . Hence, there is no CH* peak around 431 nm (Fig. 2.13) and the signal from that chemical compound was not included in Fig. 2.14. Since a diffusion flame was more stable and easier to manage, it was possible to investigate the flame for a wider range of oxygen compound than for the premixed flame. As mentioned before, for CO_2 as a diluent, for lower O_2 content, it was impossible to obtain the stable flame.

Generally, the results obtained for the diffusion flame are similar to those from the premixed one i.e. with higher oxygen content the signal is getting stronger. However, it should be emphasised that for lower oxygen content (below 55 %) the signal is almost constant, which is clearly visible in case of OH* signal coming from a flame where the oxygen was diluted in carbon dioxide. As an evaluation of the measurements, Cantera script describing opposed, diffusion flame were implemented. There were, however a serious issues that prevent form getting meaningful results. As a conclusion - for diffusion flame it is necessary to improve the Cantera software or find a
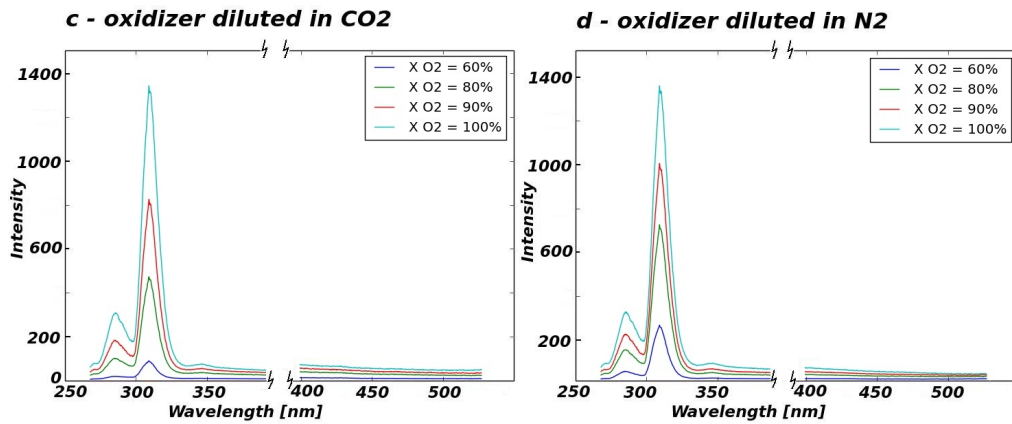
Figure 2.13: Intensity distribution for diffusion flame

suitable replacement. Other possibility is a Chemkin software commonly use in other studies [12, 14, 16].

Summarizing, OH* signal was the strongest source of photon emission in the investigated wavelength range, for both flame types and both oxidizer diluents. Hence, its measurement and potential usage in the industrial environment should be easier than application of CH* signal, especially in case of diffusion flame. Moreover, the higher value of oxygen content in the oxidizer should facilitate the chemiluminescence application.
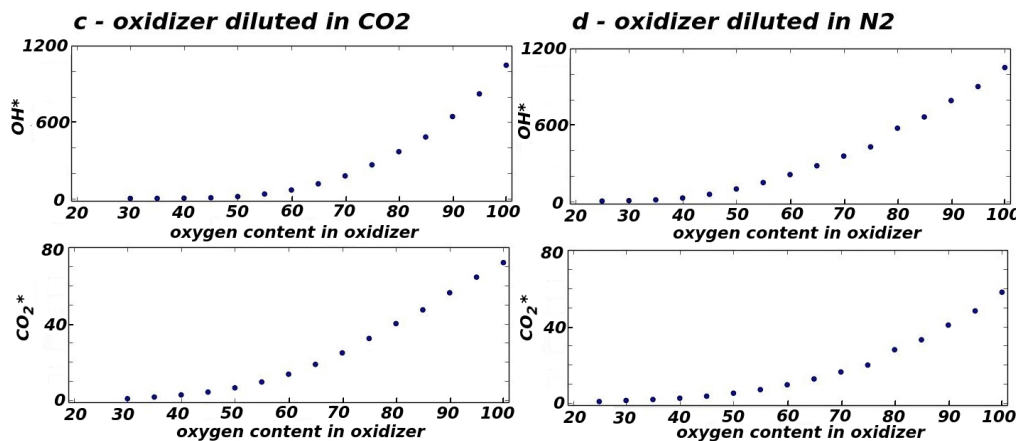
Figure 2.14: Measured signal from the excited species in the diffusion flame

3 Summary

Within the scope of the work, selected chemical kinetics and combustion issues were investigated.

The first part contains a study of high temperature plasma and its potential usage as a working fluid in the magnetohydrodynamic generator. The well established GRI 3.0 mechanism for methane combustion has been extended to include electrons and ions from literature in order to evaluate the effect of oxy-fuel combustion on the production of these, hence their potential to generate a high enough conductivity for MHD applications. The results show, however, that it is highly unlikely to obtain, in the industrial environment, naturally ionized plasma that could be applied as a working fluid in the effective MHD generator. Electron and ion concentration that defines electrical conductivity of the fluid is simply not high enough. In other words - without additional seeding that increases electrical conductivity, it would be very problematic (and expensive) for the MHD generator to function with naturally ionized combustion gasses. The pressure and temperature required to obtain naturally ionized plasma characterized by adequate parameters for the magnetohydrodynamic power plant are beyond the present industrial possibilities.

The second part describes a chemiluminescence study of the excited species in various flame types. In this section of the work the previous mechanism has been further extended to include chemiluminescence reactions for OH^*, CH^* and CO_2^* from different literature sources. The mechanism has been validated against experiments in both premixed and diffusion flame configurations. The obtained mechanism can be used to assess the potential for monitoring flames in oxy-fuel conditions. Conducted measurements proves the accuracy of the created mechanism in case of OH^*, CH^* and provides a groundwork for the future studies of chemiluminescence phenomena.

4 Scripts

This part provides an insight into the programming part of the conducted work. All the main scripts are included.

4.1 Calculations of the plasma electrical conductivity

```python
#!/usr/bin/python3.4

import cantera as ct
import csv
import matplotlib.pyplot as plt
import math

# define a mixture
mixture = ct.Solution('gri30MOD.cti')

# a file in  which the results will be written
myfile = open('equilibration_results.csv','w')
csvwriter = csv.writer(myfile)
# labels
csvwriter.writerow(['Tb, K','Ta, K','X H3O+','Y H3O+','X e-','Y e-',
                    'n_e, 1/cm3','n_e, mole/gram','\sigma_E, S/m',
                    '\sigma_H3O+, S/m', '\sigma_all, S/m'])

# initial temperaure
T = 300
dT = 100
# temperature
x1 = []
y1 = []

# the loop for calculating all of the relevant parameters
# for different initial temperatures
while T <= 1900:

    # define mixture parameters
    mixture.TP = T, 100000,
    mixture.X = 'CH4:1, O2:2'

    # initial temperature of the mixture
    Tb = mixture.T

    # mole fractions of the mixture
    mole = mixture.X

    # create the reactor, and fill it with mixture
    reactor = ct.IdealGasConstPressureReactor(mixture)
```

```python
# H3O+ and e- mole and mass fractions within the reactor
XH3O_b = reactor.thermo['H3O+'].X
YH3O_b = reactor.thermo['H3O+'].Y
print('H3O+ :','X :', XH3O_b,'Y :', YH3O_b)
Xe_b = reactor.thermo['e-'].X
Ye_b = reactor.thermo['e-'].Y
print('e- :','X :', Xe_b,'Y :', Ye_b)

# equilibriation with constant enthalpy and pressure
mixture.equilibrate('HP')

# mole fractions of the mixture
mole = mixture.X
print(mole)
print(mixture())

# create the reactor, and fill it with mixture
reactor = ct.IdealGasConstPressureReactor(mixture)

# H3O+ and e- mole and mass fractions of the reactor
XH3O_a = reactor.thermo['H3O+'].X
YH3O_a = reactor.thermo['H3O+'].Y
print('H3O+ :','X :', XH3O_a,'Y :', YH3O_a)
Xe_a = reactor.thermo['e-'].X
Ye_a = reactor.thermo['e-'].Y
print('e- :', 'X :',Xe_a, 'Y :',  Ye_a)

# CALCULATION OF ELECTRICAL CONDUCTIVITY:
Cg = mixture.density / mixture.mean_molecular_weight #(kmol/m3)

# Avagadro Constant
No = 6.022E26            #(1/kmol)
# all particles concentration
N = Cg * No             #(1/m3)

# ELECTRONS
# data:
e_e = 1.60217662E-19        #(C = A*s)  elementary charge of electron
m_e = 9.109E-31             #(kg)       mass of one electron
vN_e = 17.6E-8 * 1/1000000  #(m3/s)     effective collision frequency
                            #           of electrons in atmospheric gases
                            #           per N
```

```python
# effective collision frequency of electrons in atmospheric gases
v_e = vN_e * N                     #(1/s) or (particles / s)

# electron concentration
n_e = N * Xe_a                     #(1/m3)
print('electron concentration:',n_e/1000000,'1/cm3')

n_e_mole = n_e / (6.022E23 * mixture.density * 1000) #(mole/gram)
print('electron concentratuon:',n_e_mole,'mole/gram')

#electrical conductivity of electrons
sigma1 = ( e_e*e_e * n_e ) / ( m_e * v_e )
print('electrical conductivity E:',sigma1, '(A2 * s3)/(kg * m3)')

# IONS
# data:
e_i = 1.60217662E-19       #(C = A*s)   elementary charge of electron
m_i = 3.159E-26            #(kg)        mass of the particle
vN_i = 17.6E-8 * 1/1000000 #(m3/s)      effective collision frequency ?
                           #            of electrons in atmospheric gases
                           #            per N !!!

# effective collision frequency of ions in atmospheric gases
v_i = vN_i * N                     #(1/s)

# electron concentration
n_i = N * XH3O_a                   #(1/m3)

# electrical conductivity of positive ions represented by H3O+
sigma2 = ( e_i*e_i * n_i ) / ( m_i * v_i )
print('electrical conductivity H3O+:',sigma2, '(A2 * s3)/(kg * m3)')

# total electrical conductivity
sigma = sigma1 + sigma2
print('electrical conductivity:',sigma, '(A2 * s3)/(kg * m3)')

# temperature of the mixture (after equilibriation)
Ta = mixture.T

# temperatures
x1.append(Tb)
y1.append(Ta)
```

```python
    T = T + dT

    # write calculated parameters to the csv file
    csvwriter.writerow([Tb,Ta,XH3O_a,YH3O_a,Xe_a,Ye_a,n_e/1000000,
                                    n_e_mole,sigma1,sigma2,sigma])
myfile.close()

# Temperature of the gas after equilibration as a function
# of the temperature before equilibration
fig1 = plt.figure(1)
rect1 = fig1.patch
plot1 = fig1.add_subplot(1,1,1)
plot1.plot(x1,y1)
plt.xlabel('T before eq [K]')
plt.ylabel('T after eq [K]')

plt.show()
```

4.2 Signal calibration for the visible spectrum

```python
#!/usr/bin/python3.4
import csv
import matplotlib.pyplot as plt
import math
import numpy as np
from Model_Values import I1


##############################################################################
################ VISIBLE SPECTRUM ############################################
##############################################################################
W1 = []
for i in range(171): #171
    xx1 = 250 + 5 *i
    W1.append(xx1)
# Model Range for measurements
model_L = 3
model_R = 60
x_model = W1[model_L:model_R]
y_model = I1[model_L:model_R]


################# Measured ####################################################
####### READ DATA FILE SECTION ######################################
file_directory = '/home/jb0183/Measurements/Calibration/'
file_name = 'LAMP-Heraeus-400nm-300BLZ1_1'
full_directory = file_directory + file_name + '.txt'
file1 = open(full_directory,'r')
#read all the lines
all_lines = []
with file1 as f:
    for line in f:
        inner_list = [elt.strip() for elt in line.split(',')]
        all_lines.append(inner_list)
#delete empty space in the first line (it must be done - in other case an error occurs)
del all_lines[0][-1]
#delete the first element in every list (like ,,wavelength'' ,,pixel''  etc.)
loops = len(all_lines)
for i in range(loops):
    del all_lines[i][0]
#convert list of strings to list of floats
all_lines = [[float(float(j)) for j in i] for i in all_lines]
#CLOSE TXT FILE !
file1.close()
```

```python
# Measured Range
Measured_L = 30
Measured_R = 980

x_Measured = all_lines[1][Measured_L:Measured_R]
y_Measured = all_lines[3][Measured_L:Measured_R]

# THE POINT (X axis) where two ranges meet (UV and visible)
# used for normalization
POINT = 330 #for a wavelength = 350 nm
#measured value  in a POINT
P_Measured = all_lines[3][POINT]
#model value
P_model = I1[20]
#ratio in a Point
P_ratio = P_model/P_Measured
# normalized values of y_
y_Measured_norm = [x * (P_ratio) for x in y_Measured]

############## trend line for model ##############################
#coefficients for polynomial, 4th degree
coe_model = np.polyfit(x_model,y_model,6)

#create new y values for model according to coefficients
loops = len(x_Measured)
y_model_trend = []
for i in range(loops):
    y_fit_model = coe_model[0]*math.pow(x_Measured[i],6) + coe_model[1]*math.pow(x_Measured[i],5)
    + coe_model[2]*math.pow(x_Measured[i],4) + coe_model[3]*math.pow(x_Measured[i],3)
    + coe_model[4]*math.pow(x_Measured[i],2) + coe_model[5]*x_Measured[i] + coe_model[6]
    y_model_trend.append(y_fit_model)

############## trend line for measurements ##############################
coe_Real = np.polyfit(x_Measured,y_Measured_norm,6)

#create new y values for measured values according to coefficients
loops = len(x_Measured)
y_Measured_norm_trend = []
for i in range(loops):
    y_fit_Measured = coe_Real[0]*math.pow(x_Measured[i],6) + coe_Real[1]*math.pow(x_Measured[i],5)
    + coe_Real[2]*math.pow(x_Measured[i],4) + coe_Real[3]*math.pow(x_Measured[i],3)
    + coe_Real[4]*math.pow(x_Measured[i],2) + coe_Real[5]*x_Measured[i] + coe_Real[6]
    y_Measured_norm_trend.append(y_fit_Measured)
```

```python
############## correction factor ############################

cor_fac = np.array(y_model_trend) / np.array(y_Measured_norm_trend)

data1 = open('Correction_factor_allinone.csv','w')
csvwriter1 = csv.writer(data1)
csvwriter1.writerow(x_Measured)
csvwriter1.writerow(cor_fac)

############## final list of correction values for y measured ############################

y_Measured_cor = cor_fac * np.array(y_Measured_norm)

######### CHARTS #######################################
# Model line - actual and trend line
fig1 = plt.figure(1)
plot1 = fig1.add_subplot(4,2,2)
plot1.plot(x_model,y_model)
plot2 = fig1.add_subplot(4,2,2)
plot2.plot(x_Measured,y_Measured_cor)
plt.xlabel('wavelength (nm)')
plt.ylabel('Intensity')
plot3= fig1.add_subplot(4,2,4)
plot3.plot(x_Measured,y_model_trend)
plt.xlabel('wavelength (nm)')
plt.ylabel('Intensity')

# Measured line - actual and trend line
plot4 = fig1.add_subplot(4,2,6)
plot4.plot(x_Measured,y_Measured_norm)
plt.xlabel('wavelength (nm)')
plt.ylabel('Intensity')
plot5 = fig1.add_subplot(4,2,8)
plot5.plot(x_Measured,y_Measured_norm_trend)
plt.xlabel('wavelength (nm)')
plt.ylabel('Intensity')
```

4.3 Measurement post-processing script

```python
#!/usr/bin/python3.4

####### IMPORT SECTION ##############################################

#Basic modules
import csv
import matplotlib.pyplot as plt
import math
import numpy as np
#Image module
import scipy.misc as misc
from scipy.misc import imread
from scipy.misc import imsave
#Abel module
import abel as abel
import abel.transform as transform
from abel.transform import Transform
#Integration module
import scipy.integrate as integ
from scipy.integrate import trapz
#For a nmber of files in a directory
import os, os.path
#For finding the index of the pxel charactricterized by the highest value of intensity
from numpy import unravel_index
# import calibration list for every wavelength from Calibration script
from Calibration import cor_fac

#Data:
rho_CH4 = 0.668 #kgN/m3N
rho_CO2 = 1.842 #kgN/m3N
rho_O2 = 1.331 #kgN/m3N
rho_N2 = 1.165 #kgN/m3N
M_CH4 = 16 #kg/kmol
M_CO2 = 44 #kg/kmol
M_O2 = 32 #kg/kmol
M_N2 = 28 #kg/kmol

CH4_flow = np.array([0.7, 1.3, 2.2, 3.6, 5.8, 7.1]) #Nl/min fuel and oxidizer flow is variable
ox_flow = np.array([4.2, 6.6, 10.0, 14.3, 21.1, 23.6]) #Nl/min oxidizer flow
#diameters:
r_CH4 = 0.001 #m
r_ox = 0.025 #m
# mass flows:
CH4_flow_mass_array = []
ox_flow_mass_array = []
```

```python
#oxidizer content
ox_cont_array =  []
# SIGNALS
OH_signal_array = []
CH_signal_array = []
CO2_signal_array = []
#mole fractions:
n_frCH4_array = []
n_frO2_array = []
n_frN2_array = []
n_frCO2_array = []
#Mass flows of fuel and oxidizer:
CH4_flow_mass_array = []
ox_flow_mass_array = []
#choose CO2 or N2 (air) as a diluent of oxygen
Marker = 'N2'

#file directory
if Marker == 'N2':
    file_directory = '/home/jb0183/Measurements/Results/Premixed_N2/'
if Marker == 'CO2':
    file_directory = '/home/jb0183/Measurements/Results/Premixed_CO2/NEW/'

number_of_files = len([name for name in os.listdir(file_directory)
if os.path.isfile(os.path.join(file_directory, name))])

My_range = number_of_files - 1 #minus 1 file with other data
ox_start = 35 #starting value of the oxidizer content
for i in range(My_range):
    ox_cont = ox_start + 5*i
    ox_cont_array.append(ox_cont)
    print(ox_cont)
    if Marker == 'N2':
        file_name = '1premixed-N2-' + str(ox_cont) + '_1'
    if Marker == 'CO2':
        file_name = 'KGpremixed' + str(ox_cont) + '_1'

    #mass flow of CH4
    CH4flow_mass = CH4_flow[i] * (1/60) * (1/1000) * rho_CH4 #(kg/s)
    CH4_flow_mass_array.append(CH4flow_mass)

    #mass flow of O2
    O2_flow = (ox_cont/100) * ox_flow[i]
    O2flow_mass = O2_flow * (1/60) * (1/1000) * rho_O2 #(kg/s)
```

```python
if Marker == 'N2':
    #mass flow of N2

    N2_flow = (1-(ox_cont/100)) * ox_flow[i]
    N2flow_mass = N2_flow * (1/60) * (1/1000) * rho_N2 #(kg/s)

    #mass fractions
    mfrCH4 = CH4flow_mass/(O2flow_mass + N2flow_mass + CH4flow_mass)
    mfrO2 = O2flow_mass/(O2flow_mass + N2flow_mass + CH4flow_mass)
    mfrN2 = N2flow_mass/(O2flow_mass + N2flow_mass + CH4flow_mass)

    #mole fraction
    nfrCH4 = (mfrCH4/M_CH4) / (mfrO2/M_O2 + mfrN2/M_N2 + mfrCH4/M_CH4)
    nfrO2 = (mfrO2/M_O2) / (mfrO2/M_O2 + mfrN2/M_N2 + mfrCH4/M_CH4)
    nrfN2 = (mfrN2/M_N2) / (mfrO2/M_O2 + mfrN2/M_N2 + mfrCH4/M_CH4)
    n_frCH4_array.append(nfrCH4)
    n_frO2_array.append(nfrO2)
    n_frN2_array.append(nrfN2)

    #######################

    #density of oxidizer:
    rho_ox = (ox_cont/100) * rho_O2 + (1 - (ox_cont/100)) * rho_N2
    #mass flow of oxidizer:
    ox_flow_mass = ox_flow[i] * (1/60) * (1/1000) * rho_ox * 1/(3.14*(math.pow(r_ox,2))) #(kg/m^2/s)
    ox_flow_mass_array.append(ox_flow_mass)

if Marker == 'CO2':
    #mass flow of CO2
    CO2_flow = (1-(ox_cont/100)) * ox_flow[i]
    CO2flow_mass = CO2_flow * (1/60) * (1/1000) * rho_CO2 #(kgN/s)

    #mass fraction
    mfrCH4 = CH4flow_mass/(O2flow_mass + CO2flow_mass + CH4flow_mass)
    mfrO2 = O2flow_mass/(O2flow_mass + CO2flow_mass + CH4flow_mass)
    mfrCO2 = CO2flow_mass/(O2flow_mass + CO2flow_mass + CH4flow_mass)

    #mole fraction
    n_frCH4 = (mfrCH4/M_CH4) / (mfrO2/M_O2 + mfrCO2/M_CO2 + mfrCH4/M_CH4)
    n_frO2 = (mfrO2/M_O2) / (mfrO2/M_O2 + mfrCO2/M_CO2 + mfrCH4/M_CH4)
    n_rfCO2 = (mfrCO2/M_CO2) / (mfrO2/M_O2 + mfrCO2/M_CO2 + mfrCH4/M_CH4)
    n_frCH4_array.append(n_frCH4)
    n_frO2_array.append(n_frO2)
    n_frCO2_array.append(n_rfCO2)
```

```python
    #density of oxidizer:
    rho_ox   = (ox_cont/100) * rho_O2 + (1 - (ox_cont/100)) * rho_CO2
    #mass flow of oxidizer:
    ox_flow_mass = ox_flow * (1/60) * (1/1000) * rho_ox * 1/(3.14*(math.pow(r_ox,2))) #(kg/m^2/s)
    ox_flow_mass_array.append(ox_flow_mass)

###### USER'S DATA SECTION ########################################
if Marker == 'CO2':
    #define image size (physical dimension) - number of pixels should be odd
    Left = 74
    Right = 171

if Marker == 'N2':
    #define image size (physical dimension) - number of pixels should be odd
    Left = 70
    Right = 181 + 20

###### READ DATA FILE SECTION #####################################
full_directory = file_directory + file_name + '.txt'
file1 = open(full_directory,'r')
#read all the lines
all_lines = []
with file1 as f:
    for line in f:
        inner_list = [elt.strip() for elt in line.split(',')]
        all_lines.append(inner_list)
#delete empty space in the first line (it must be done - in other case an error occurs)
del all_lines[0][-1]
#delete the first element in every list
loops = len(all_lines)
for i in range(loops):
    del all_lines[i][0]
#convert list of strings to list of floats
all_lines = [[float(float(j)) for j in i] for i in all_lines]
#CLOSE TXT FILE !
file1.close()

######### PREPARE X VALUES ########################################
# creat a list of values for X axis (wavelength) - to cut off ,,dead area''
cut_L = 30
cut_R = 980
x1 = all_lines[1][cut_L:cut_R]
```

```python
if Marker == 'CO2':
    ###################### OH ######################
    #summing pixel arrays
    y_up_OH = 8
    y_down_OH = 30
    # prepare intensity values (taking into account calibration by correction factor)
    y1_OH = cor_fac * np.array((np.sum(Choose_Image[y_up_OH:y_down_OH], axis = 0)[cut_L:cut_R]))
    ###################### CH ######################
    #summing pixel arrays
    y_up_CH = 17
    y_down_CH = 39
    y1_CH = cor_fac * np.array((np.sum(Choose_Image[y_up_CH:y_down_CH], axis = 0)[cut_L:cut_R]))
    ###################### CO2 ######################
    y1_CO2 = y1_CH
if Marker == 'N2':
    ###################### OH ######################

    y_up_OH = 14
    y_down_OH = 35
    # prepare intensity values (taking into account calibration by correction factor)
    y1_OH = cor_fac * np.array((np.sum(Choose_Image[y_up_OH:y_down_OH], axis = 0)[cut_L:cut_R]))
    ###################### CH ######################

    y_up_CH = 24
    y_down_CH = 42
    y1_CH = cor_fac * np.array((np.sum(Choose_Image[y_up_CH:y_down_CH], axis = 0)[cut_L:cut_R]))

############ Intensity charts ############
### limits for Intensity and integration charts ###
X_lim_L = 250
X_lim_R = 550
###### final chart - half from OH range, half from CH and CO2 range  ##########
y1_final = list( y1_OH[:(len(y1_OH)/2)] ) + list( y1_CH[(len(y1_CH)/2):] )
y1_final = [x/1000 for x in y1_final]
plot3 = fig1.add_subplot(1,1,1)
plot3.plot(x1,y1_final,label = 'X O2 = ' + str(ox_cont) + '%')
#plt.title('CH and CO2 signal', fontsize=12, fontweight='bold')
plt.xlabel('Wavelength (nm)')
plt.ylabel('Intensity')
plt.ylim([0,(max(y1_final) + 0.12 * max(y1_final))])
plt.xlim([X_lim_L,X_lim_R])
plt.legend()
plt.savefig('Complete_signal' + Marker + '.jpeg')
```

```python
####### SAVE TO CSV ###############
data1 = open('Intensity as a function' + str(ox_cont) + 'of a wavelength.csv','w')
csvwriter1 = csv.writer(data1)
csvwriter1.writerow(x1)
csvwriter1.writerow(y1_final)
data1.close()

####### INTEGRATION FUNCTION #################################################
def Integration (int_L,int_R,y1):

    #integrated part of the signal
    x1_int = all_lines[1][int_L:int_R]
    y1_int = y1[int_L:int_R]
    #integration of the signal with background
    int_all = trapz(np.array(y1_int),np.array(x1_int))

    ############## trend line to cut off the bottom #####################
    #range as a basis for trend line
    LeftL = int_L - 70
    LeftR = int_L # left side of integration range
    RighrL = int_R # right side of integration range
    RightR = int_R + 70
    x1_base_tr = np.array(all_lines[1][LeftL:LeftR] + all_lines[1][RighrL:RightR])
    y1_base_tr = np.array(list(y1[LeftL:LeftR]) + list(y1[RighrL:RightR]))

    #coefficients for polynomial, 4th degree
    coe_tr = np.polyfit(x1_base_tr,y1_base_tr,6)

    #create y_cutoff values for model according to coefficients
    loops = len(x1_int)
    y_cutoff = []
    for i in range(loops):
        y_fit_model = coe_tr[0]*math.pow(x1_int[i],6) + coe_tr[1]*math.pow(x1_int[i],5)
        + coe_tr[2]*math.pow(x1_int[i],4) + coe_tr[3]*math.pow(x1_int[i],3)
        + coe_tr[4]*math.pow(x1_int[i],2) + coe_tr[5]*x1_int[i] + coe_tr[6]
        y_cutoff.append(y_fit_model)

    # integration with cutted area
    int_cutoff = trapz(np.array(y_cutoff),np.array(x1_int))

    #signal - area of total signal minus background
    signal = int_all - int_cutoff

    return(signal, x1_int, y1_int, x1_base_tr, y1_base_tr, y_cutoff, int_all)
```

```python
###### OH  #################################################
#range  - the range is moved to the right by ,,cut_L'' value
OH_L = 145 - cut_L
OH_R = 220 - cut_L
OH_data = Integration(OH_L,OH_R,y1_OH)
OH_signal_array.append(OH_data[0])
print('OH  signal',OH_data[0])


###### CH  #################################################
CH_L = 590 - cut_L
CH_R = 660 - cut_L
CH_data = Integration(CH_L,CH_R,y1_CH)
CH_signal_array.append(CH_data[0])
print('CH  signal',CH_data[0])


###### CO2  #################################################

CO2_L = 540 - cut_L
CO2_R = 580 - cut_L
CO2_data = Integration(CO2_L,CO2_R,y1_CO2)
CO2_signal_array.append(CO2_data[6])
print('CO2  signal',CO2_data[6])

#INTEGRATION CHECK

### OH ###
fig100 = plt.figure(100)
plot1 = fig100.add_subplot(1,1,1)
plot1.plot(OH_data[1],OH_data[2])
plot2 = fig100.add_subplot(1,1,1)
plot2.plot(OH_data[3],OH_data[4])
plot3 = fig100.add_subplot(1,1,1)
plot3.plot(OH_data[1],OH_data[5])

### CH ###
plot4 = fig100.add_subplot(1,1,1)
plot4.plot(CH_data[1],CH_data[2])
plot5 = fig100.add_subplot(1,1,1)
plot5.plot(CH_data[3],CH_data[4])
plot6 = fig100.add_subplot(1,1,1)
plot6.plot(CH_data[1],CH_data[5])
```

```python
### CO2 ###
plot7 = fig100.add_subplot(1,1,1)
plot7.plot(CO2_data[1],CO2_data[2])

plt.xlabel('Wavelength (nm)')
plt.ylabel('Intensity')
plt.ylim([0,(max(OH_data[2]) + 0.12 * max(OH_data[2]))])
plt.xlim([X_lim_L,X_lim_R])

#plt.show()

xlim = ( min(ox_cont_array) - 1 ),( max(ox_cont_array) + 1 )

fig3 = plt.figure(3)
plot1 = fig3.add_subplot(3,1,1)
plot1.scatter(ox_cont_array[0:My_range],OH_signal_array)
plt.xlabel('Oxygen content in oxidizer')
plt.ylabel('OH signal')
plt.xlim(xlim)
plt.ylim([0,(max(OH_signal_array) + 0.1 * max(OH_signal_array))])
plot2 = fig3.add_subplot(3,1,2)
plot2.scatter(ox_cont_array[0:My_range],CH_signal_array)
plt.xlabel('Oxygen content in oxidizer')
plt.ylabel('CH signal')
plt.xlim(xlim)
plt.ylim([0,(max(CH_signal_array) + 0.1 * max(CH_signal_array))])
plot3 = fig3.add_subplot(3,1,3)
plot3.scatter(ox_cont_array[0:My_range],CO2_signal_array)
plt.xlabel('Oxygen content in oxidizer')
plt.ylabel('CO2 signal')
plt.xlim(xlim)
plt.ylim([0,(max(CO2_signal_array) + 0.1 * max(CO2_signal_array))])
plt.savefig('MEASUREMENTS_' + Marker + '.jpeg')

plt.show()
```

4.4 Measurement evaluation

```python
#!/usr/bin/python3.4
"""
A freely-propagating, premixed hydrogen flat flame with multicomponent
transport properties.
"""
import cantera as ct
import numpy as np
import math

import csv
import matplotlib.pyplot as plt

#Integration module
import scipy.integrate as integ
from scipy.integrate import trapz
#import mole fractions from measurement
from KG_premixed import n_frCH4_array
from KG_premixed import n_frO2_array
from KG_premixed import n_frN2_array
from KG_premixed import n_frCO2_array
#importoxygen content from measurement
from KG_premixed import ox_cont_array
# The main goal - calculated OH and CH signal
int_OH_rate_array = []
int_CH_rate_array = []
int_CO2_rate_array = []
int_CO2_rate_array_OLD = []
# For final charts
from KG_premixed import OH_signal_array
from KG_premixed import CH_signal_array
from KG_premixed import CO2_signal_array
from KG_premixed import Marker #CO2 or N2
from KG_premixed import My_range #number of loops

for i in range(My_range):
    CH4 = str(n_frCH4_array[i])
    O2 = str(n_frO2_array[i])
    if Marker == 'N2':
        N2 = str(n_frN2_array[i])
    if Marker == 'CO2':
        CO2 = str(n_frCO2_array[i])

    MECHANISM = 'gri30LUMpremixed_ALL'
```

```python
# Simulation parameters
p = 101325  # pressure [Pa]
Tin = 300.0  # unburned gas temperature [K]
if Marker == 'N2':
    reactants = 'CH4:'+ CH4 + ',' + 'O2:' + O2 + ',' + 'N2:' + N2  # premixed gas composition
if Marker == 'CO2':
    reactants = 'CH4:'+ CH4 + ',' + 'O2:' + O2 + ',' + 'CO2:' + CO2  # premixed gas composition
print(reactants)

initial_grid = np.linspace(0.0, 0.03, 7)  # m ; number of points on the axis ; range
tol_ss = [1.0e-5, 1.0e-13]  # [rtol atol] for steady-state problem
tol_ts = [1.0e-4, 1.0e-13]  # [rtol atol] for time stepping
loglevel = 1  # amount of diagnostic output (0 to 8)
refine_grid = True  # 'True' to enable refinement, 'False' to disable

# IdealGasMix object used to compute mixture properties, set to the state of the
# upstream fuel-air mixture



gas = ct.Solution(MECHANISM + '.xml')
gas.TPX = Tin, p, reactants

# Flame object
f = ct.FreeFlame(gas, initial_grid)
f.flame.set_steady_tolerances(default=tol_ss)
f.flame.set_transient_tolerances(default=tol_ts)

f.show_solution()

# Solve with the energy equation disabled
f.energy_enabled = False
f.transport_model = 'Mix'
f.set_max_jac_age(10, 10)
f.set_time_step(1e-5, [2, 5, 10, 20])
f.solve(loglevel=loglevel, refine_grid=False)
f.save('h2_adiabatic.xml', 'no_energy',
       'solution with the energy equation disabled')

# Solve with the energy equation enabled
f.set_refine_criteria(ratio=3, slope=0.06, curve=0.12)
f.energy_enabled = True
f.solve(loglevel=loglevel, refine_grid=refine_grid)
f.save('h2_adiabatic.xml', 'energy',
       'solution with mixture-averaged transport')
```

```python
f.show_solution()
print('mixture-averaged flamespeed = {0:7f} m/s'.format(f.u[0]))

# Solve with multi-component transport properties
f.transport_model = 'Multi'
f.solve(loglevel, refine_grid)
f.show_solution()
print('multicomponent flamespeed = {0:7f} m/s'.format(f.u[0]))
f.save('h2_adiabatic.xml','energy_multi',
        'solution with multicomponent transport')

# write the velocity, temperature, density, and mole fractions to a CSV file
f.write_csv('h2_adiabatic.csv', quiet=False)

#charts
#data:
grid1 = f.grid
rate347 = f.forward_rates_of_progress[346]
rate348 = f.forward_rates_of_progress[347]
OHex = f.concentrations[53]
CHex = f.concentrations[54]

#if MECHANISM == 'gri30LUMpremixed_ALL':
rate362 = f.forward_rates_of_progress[361]

fig2 = plt.figure(2)
plot1 = fig2.add_subplot(1,1,1)
plot1.plot(grid1,rate362)
plt.title('rate 362')

#write to a file
myfile = open('Oposed_check_results.csv','w')
csvwriter = csv.writer(myfile)
csvwriter.writerow(grid1)
csvwriter.writerow(f.forward_rates_of_progress[347])
csvwriter.writerow(f.concentrations[54])
myfile.close()

fig1 = plt.figure(1)
plot1 = fig1.add_subplot(2,2,1)
plot1.plot(grid1,rate347)
plt.title('net rate R347')
plt.xlim([0.01,0.015])
plot2 = fig1.add_subplot(2,2,2)
plot2.plot(grid1,rate348)
```

```python
        plot3 = fig1.add_subplot(2,2,3)
        plot3.plot(grid1,CHex)
        plt.title('CHex')
        plt.xlim([0.01,0.015])
        plot4 = fig1.add_subplot(2,2,4)
        plot4.plot(grid1,CHex)
        plt.title('OHex')
        plt.xlim([0.01,0.015])

        #plt.show()

        int_OH_rate = trapz(np.array(rate348),np.array(grid1))
        int_OH_rate_array.append(int_OH_rate)
        int_CH_rate = trapz(np.array(rate347),np.array(grid1))
        int_CH_rate_array.append(int_CH_rate)

        int_CO2_rate = trapz(np.array(rate362),np.array(grid1))
        int_CO2_rate_array.append(int_CO2_rate)

xlim = ( min(ox_cont_array) - 1 ),( max(ox_cont_array) + 1 )

### FINAL ###
factor = 0.0001

# OH #
# adjust the trendline to measured points
rate_OH = max(OH_signal_array) / max(int_OH_rate_array)
int_OH_rate_array = [x*rate_OH*0.95 for x in int_OH_rate_array]
# lower the value by the factor
OH_signal_array = [x*factor for x in OH_signal_array]
int_OH_rate_array = [x*factor for x in int_OH_rate_array]

fig5 = plt.figure(5)
plot1 = fig5.add_subplot(3,1,1)
plot1.scatter(ox_cont_array[0:My_range],OH_signal_array, label = 'measurements')
plot2 = fig5.add_subplot(3,1,1)
plot2.plot(ox_cont_array[0:(My_range)],int_OH_rate_array, color = '0.5')
plot21 = fig5.add_subplot(3,1,1)
plot21.scatter(ox_cont_array[0:(My_range)],int_OH_rate_array, marker = 'h', color = '0.5', label = 'calculations')
plt.xlabel('Oxygen content in oxidizer')
plt.ylabel('OH signal')
plt.xlim(xlim)
plt.ylim([0,80])
```

```python
# CH #
rate_CH = max(CH_signal_array) / max(int_CH_rate_array)
int_CH_rate_array = [x*rate_CH*0.95 for x in int_CH_rate_array]

CH_signal_array = [x*factor for x in CH_signal_array]
int_CH_rate_array = [x*factor for x in int_CH_rate_array]

plot3 = fig5.add_subplot(3,1,2)
plot3.scatter(ox_cont_array[0:My_range],CH_signal_array, label = 'measurements')
plot4 = fig5.add_subplot(3,1,2)
plot4.plot(ox_cont_array[0:(My_range)],int_CH_rate_array, color = '0.5')
plot41 = fig5.add_subplot(3,1,2)
plot41.scatter(ox_cont_array[0:(My_range)],int_CH_rate_array, marker = 'h', color = '0.5')
plt.xlabel('Oxygen content in oxidizer')
plt.ylabel('CH signal')
plt.xlim(xlim)
plt.ylim([0,6])

# CO2 #
rate_CO2 = max(CO2_signal_array) / max(int_CO2_rate_array)
int_CO2_rate_array = [x*rate_CO2*1.05 for x in int_CO2_rate_array]

rate_CO2 = max(CO2_signal_array) / max(int_CO2_rate_array_OLD)
int_CO2_rate_array_OLD = [x*rate_CO2*1.05 for x in int_CO2_rate_array_OLD]

CO2_signal_array = [x*factor for x in CO2_signal_array]
int_CO2_rate_array = [x*factor for x in int_CO2_rate_array]
int_CO2_rate_array_OLD = [x*factor for x in int_CO2_rate_array_OLD]

plot5 = fig5.add_subplot(3,1,3)
plot5.scatter(ox_cont_array[0:My_range],CO2_signal_array)
plot6 = fig5.add_subplot(3,1,3)
plot6.plot(ox_cont_array[0:(My_range)],int_CO2_rate_array, color = '0.5')
plot61 = fig5.add_subplot(3,1,3)
plot61.plot(ox_cont_array[0:(My_range)],int_CO2_rate_array, marker = 'h', color = '0.5') #, label = 'mechanism')
plt.xlabel('Oxygen content in oxidizer')
plt.ylabel('CO2 signal')
plt.xlim(xlim)
plt.ylim([0,10])
plt.legend(loc = '2')
plt.savefig('FINAL_ALL' + Marker + '.jpeg')
print(int_CO2_rate_array_OLD)
plt.show()
```

References

[1] Steven Errede. 2007. A Brief History of The Development of Classical Electrodynamics.

[2] Carl-W. Hustad, David L. Coleman, Tom Mikus. 2009. Technology Overview for Integration of an MHD Topping Cycle with the CES Oxyfuel Combustor.

[3] Fernandorueda Rueda Martnez, Aldo Antonio Rueda Martnez, Miguel Toledo Velzquez, Pedro Quinto Diez, Guilibaldo Tolentino Eslava, Juan Abugaber Francis. 2011. Evaluation of the Gas Turbine Inlet Temperature with Relation to the Excess Air.

[4] E.P. Velikhov, R.V. Dogadaev, V.P. Panchenko, A.A. Yakushev b , B.V. Kononov, Yu.M. Milekhin, and N.N. Parfenov. 2010. Study of Properties of Combustion Products of Advanced Solid Plasma Generating Propellant for Pulsed MHD Generators.

[5] Sufia Khalili, Ali Jafarian Dehkordi, Mohammad Hossein Giahi. 2014. Investigating the effect of channel angle of a subsonic MHD (Magneto-Hydro-Dynamic) generator on optimum efficiency of a triple combined cycle.

[6] Naoyuki Kayukawa. 2002. Open-cycle magnetohydrodynamic electrical power generation: a review and future perspectives.

[7] Memdouh Belhi, Pascale Domingo, Peirre Vervisch. 2010. Direct numerical simulation of the effect of an electric field on flame stability.

[8] Bonnie J. McBride, Sanford Gordon, Martin A. Reno. 1993. Coefficients for Calculating Thermodynamic and Transport Properties of Individual Species. National Aeronautics and Space Administration.

[9] Fernandorueda Rueda Martnez, Aldo Antonio Rueda Martnez, Miguel Toledo Velzquez, Pedro Quinto Diez, Guilibaldo Tolentino Eslava, Juan Abugaber Francis. 2011. Evaluation of the Gas Turbine Inlet Temperature with Relation to the Excess Air.

[10] Yukikazu Itikawa. 1970. Effective collision frequency of electrons in atmospheric gases.

[11] C.J.Harris, C.H.Marston, W.R.Warren. 1966. MHD Generator and Accelerator Experiments in Seeded and Unseeded Air Flows.

[12] Maurizio De Leo, Alexei Saveliev, Lawrence A. Kennedy, Serguei A. Zelepouga. 2007. OH and CH luminescence in opposed flow methane oxy-flames.

[13] Mario Ditaranto, Jorgen Hals. 2016. Combustion instabilities in sudden expansion oxy-fuel flames.

[14] Venkata Nori, Jerry Seitzman. 2008. Evaluation of Chmeliluminescence as a Combustion Diagnostic under Varying Operating Conditions.

[15] Madleine M. Kopp, Olivier Mathieu, Eric L. Petersen. 2014. Rate Determination of the CO2* Chemiluminescence Reaction $CO + O + M \leftrightarrow CO2* + M$.

[16] Tatiana Garcia-Armingol, Javier Ballester. 2014. Influence of fuel composition on chemiluminescence emission in premixed flames of $CH_4/CO_2/H_2/CO$ blends.

[17] Eric Petersen, Madleine Kopp, Nicole Donato. 2011. Assessment of Current Chemiluminescence Kinetics Models at Engine Conditions.